

Chandra X-ray Analysis of Herbig Ae/Be Stars

Hema Anilkumar,¹★ Blesson Mathew,¹ V. Jithesh,¹ Sreeja S. Kartha,¹ P. Manoj,² Mayank Narang³
and Mahathi Chavali,⁴

¹Department of Physics & Electronics, CHRIST (Deemed to be University), Bangalore 560029, India

²Department of Astronomy and Astrophysics, Tata Institute of Fundamental Research Homi Bhabha Road, Colaba, Mumbai 400005, India

³Academia Sinica Institute of Astronomy & Astrophysics, 11F of Astro-Math Bldg., No. 1, Sec. 4, Roosevelt Road, Taipei 10617, Taiwan, Republic of China

⁴Max Planck Institute for Radio Astronomy, Auf dem Hügel 69, 53121 Bonn, Germany

Accepted XXX. Received YYY; in original form ZZZ

ABSTRACT

Herbig Ae/Be (HAeBe) stars are intermediate-mass pre-main sequence stars, characterized by infrared excess and emission lines. They are observed to emit X-rays, whose origin is a matter of discussion and not settled yet. X-ray emission is not expected in HAeBe stars, as they lack the sub-surface convective zone. In this study, we retrieved observations from the *Chandra* archive for 62 HAeBe stars, among which 44 sources (detection fraction $\sim 71\%$) were detected in X-rays, with 7 being new detections. We use this sample as a test bed to conduct a comparative analysis of the X-ray properties of HAeBe stars and their low-mass counterparts, T Tauri Stars (TTs). Further, we compare the X-ray properties of HAeBe stars and TTs with optical and IR properties to constrain the X-ray emission mechanism in HAeBe stars. We found no correlation between X-ray emission and disk properties of HAeBe stars, confirming that X-rays are not related to accretion shocks. About 56% of HAeBe stars without any known sub-arcsec companions have lower plasma temperatures ($kT \leq 2$ keV). We observe flaring/variability in HAeBe stars with confirmed low-mass companions. These stars show plasma temperatures > 2 keV, similar to TTs. Guided by this information we discuss the role of a T Tauri companion for X-ray emission seen in our sample of HAeBe stars. From the results obtained in this paper, we suggest that X-ray emission from HAeBe stars may not be related to accretion shocks or hidden TTs, but rather can be due to magnetically driven coronal emission.

Key words: stars: coroneae – stars: flare – stars: low-mass – stars: massive – stars: pre-main-sequence – techniques: imaging spectroscopy

1 INTRODUCTION

Herbig Ae/Be (HAeBe) stars are intermediate mass ($2M_{\odot} \leq M_{\star} \leq 8M_{\odot}$) young stellar objects. They are the higher mass counterparts of the T Tauri stars (TTS) (e.g., [Brittain et al. 2023](#)). Like TTSs, HAeBe stars also show $H\alpha$ emission and infrared (IR) excess from a dusty circumstellar material. In addition to this, they are also observed to emit UV and X-rays ([Zinnecker & Preibisch 1994](#); [Damiani et al. 1994](#); [Malfait et al. 1998](#)). The high energy radiation in low-mass main-sequence (MS) stars and pre-main-sequence (PMS) stars is produced predominantly due to the involvement of the magnetic field. However, the subsurface convection zone required for the production of magnetic field (through α - ω dynamo mechanism) is lacking in HAeBe stars and hence the reason for high energy emission is an unsettled problem ([Appenzeller 1994](#); [Mayne et al. 2007](#); [Mayne 2010](#)).

Many studies have been carried out to understand the origin of X-rays from HAeBe stars. Some of the initial studies to understand the origin of X-ray emission from HAeBe stars were performed by [Zinnecker & Preibisch \(1994\)](#), [Damiani et al. \(1994\)](#), [Skinner et al. \(2004\)](#) and [Hamaguchi et al. \(2005\)](#) using observations from *ASCA*, *ROSAT*, and *Einstein X-ray Observatory*. These studies could not

provide a proper explanation for the origin of X-rays in HAeBe stars due to the limited resolution of the telescope. The advent of the *Chandra X-ray Observatory* (CXO) in 1999 opened a new window (thanks to its high spatial resolution) for studying X-rays from stars. [Stelzer et al. \(2006\)](#) studied a sample of 17 HAeBe stars, of which 13 of them were X-ray emitters. Based on the high plasma temperature obtained from the spectral analysis, this study ruled out radiative winds as the sole emission mechanism and suggested that either a huge fraction of HAeBe stars are intrinsic X-ray emitters or most of the companions to HAeBe stars are yet to be discovered. [Hamidouche et al. \(2008\)](#) studied a sample of 22 HAeBe stars observed with *Chandra* and found X-ray emission from 14 stars, i.e., the sample has a detection rate of $\sim 64\%$. They found the X-ray luminosity to be higher than that of TTSs ($10^{30} - 10^{31}$ erg s^{-1}). Comparing the X-ray properties to other stellar parameters they suggested that the X-ray emission might be intrinsic to HAeBe stars, generated due to star-disk magnetic interaction. Further, [Stelzer et al. \(2009a\)](#) studied a sample of 9 HAeBe stars using the CXO with a detection rate of $\sim 100\%$. Confirming the results obtained from [Stelzer et al. \(2006\)](#), [Stelzer et al. \(2009a\)](#) suggested that unresolved (multiple stars not resolved in *Chandra*) coronally active low-mass companions as the possible reason for X-ray emission in HAeBe stars. [Nuñez et al. \(2021\)](#) studied a small sample of radiative intermediate-mass PMS (R-IMPS) stars

★ E-mail: hema.anilkumar@res.christuniversity.in

and AB-type stars and suggested a similar explanation as [Stelzer et al. \(2006, 2009a\)](#) for the emission of X-rays in HAeBe stars.

In this work, we present the results obtained by analyzing a sample of HAeBe stars showing X-ray emission and evaluate the possible mechanisms for X-ray emission. Though X-ray emission in TTSs and HAeBe stars has been studied previously, a comparative study with a large sample has not been done, especially with the data from a telescope such as *Chandra* which has an excellent sub-arcsec spatial resolution ([Tsunemi et al. 2001](#)). The paper is structured as follows: the details about the data sample of HAeBe stars and TTSs considered for this study are described in Section 2. Section 3 describes the data acquisition process and analysis of the X-ray spectra and lightcurves. Section 4 provides a detailed description of the observed X-ray properties of our sample of HAeBe stars and TTSs in the ONC. Further, the X-ray properties of HAeBe stars and TTSs are compared with their IR and optical properties. In Section 5, we discuss the role of binaries to understand the X-ray emission from HAeBe stars and explore the possible X-ray emission mechanisms in the light of our study. The main results from this study are concluded in Section 6.

2 SAMPLE

2.1 *Chandra* data of HAeBe stars

We searched for the X-ray observations in the "*Chandra Data Archive*" with a list of 279 HAeBe stars compiled from [Hamaguchi et al. \(2005\)](#), [Stelzer et al. \(2006\)](#), [Manoj et al. \(2006\)](#), [Hamidouche et al. \(2008\)](#), [Stelzer et al. \(2009a\)](#), [Chen et al. \(2016\)](#), [Vioque et al. \(2018\)](#), and identified X-ray observations for 62 HAeBe stars in the field of view (FOV) of Advanced CCD Imaging Spectrometer (ACIS) of *Chandra*. 19 of the 62 sources are presented for the first time in this paper. They are marked with "*" in Table A1. 7 of these 19 sources show X-ray emission. 28 of the 62 sources have multi-epoch data. In this paper, for spectral analysis, we consider the observation with the highest exposure and maximum number of counts for stars having multi-epoch data. We also study the temporal behavior of the stars with multi-epoch observations. Of the 62 observations corresponding to 62 sources, 44 are detected in X-rays. Our sample contains a mixture of single and multiple-star systems. The ACIS images of the 44 sources can be classified into 3 categories, i.e., resolved HAeBe star systems (11), unresolved HAeBe star systems (14), and single HAeBe stars (19). We discuss the multiple-star systems to understand the X-ray emission from HAeBe stars and rule out the possibility of TTSs being solely responsible for the observed X-ray emission. Other stellar parameters and the extinction (A_V) along the line of sight are compiled from the literature and tabulated together in Table A1. Table A1 also provides details on the X-ray status of the source, i.e., the sources detected in X-rays are denoted using "X". The multiple systems resolved by *Chandra* are denoted using "X2". The distances for all the sources are taken from the GAIA EDR3 distance catalog by [Bailer-Jones et al. \(2021\)](#).

2.2 COUP catalog : T Tauri Stars

The data for TTSs were compiled from the COUP survey program ([Getman et al. 2005](#)). The COUP program is the deepest and longest X-ray observation ever made of a young stellar cluster providing a rich and unique data set for a wide range of science studies (e.g., [Getman et al. 2005](#); [Preibisch et al. 2005](#); [Preibisch & Feigelson 2005](#); [Stelzer et al. 2005](#)). The CXO was pointed at ONC between 8 January 2003

and 21 January 2003 using the imaging configuration of the ACIS-I, which gives a FOV of $17' \times 17'$. The total exposure time of the COUP image was 838 ks, corresponding approximately to 9.7 days. The spatial resolution of ACIS is better than $1''$ over most of the FOV. The very low background allows the reliable detection of sources with as little as ~ 5 source counts. The final COUP source catalog lists 1616 individual X-ray sources. The ACIS-I chip has a very good point-spread function and a high accuracy of the aspect solution which allows for a clear and unambiguous identification of nearly all X-ray sources with optical or near-infrared counterparts ([Preibisch et al. 2005](#)). We cross-matched the sources from the COUP catalog ([Getman et al. 2005](#)), whose X-ray luminosities are available, with the optical catalog from [Da Rio et al. \(2012\)](#) and obtained around 900 sources. The cross-matched list was further filtered to contain only those sources having a membership probability $\geq 50\%$. These sources are considered to be the *bona fide* members of ONC, thereby reducing the sample size to 716. The number of known populations of stellar cluster members with precisely determined properties significantly increased in this study. So, the number of X-ray emitting TTSs in the sample considered here is more than those listed in [Preibisch et al. \(2005\)](#).

3 X-RAY DATA REDUCTION AND ANALYSIS

The data reduction was carried out using the CIAO ([Fruscione et al. 2006](#)) software package version 4.13, in combination with the calibration database (CALDB)¹ 4.9.4. We followed the standard data analysis procedure recommended by the *Chandra X-ray Center (CXC)*². The raw observation files from the archive are reprocessed to obtain the new level-2 event file, which applies the latest calibration and cleans the event file for good time intervals (GTI), removing any spurious or bright pixels (cosmic ray). We then apply an energy filter of 0.3 – 8 keV to this event file, which is the final event file used for all the scientific analyses. Further, we check for any flaring events in the background lightcurve of the observations. If present then, we follow the standard procedure as recommended by the CXC² to remove the time bins during which the flaring occurred. This is performed to keep the data uncontaminated due to the background flares. We used the source detection algorithm "wavdetect" ([Freeman et al. 2002](#)), as it is well suited for separating closely spaced point sources. The wavelet scales are set between 1 and 16 in steps of 2^n (where, $n = 0, 1, 2, 3, 4$), and a detection significance of 10^{-6} is set to avoid spurious or false detections. This threshold is lowered to 10^{-4} for the stars with the closest companions ([Stelzer et al. 2009a](#)). The position (RA & Dec) of the sources was then set to the value obtained from the "wavdetect" algorithm. We then extract the lightcurves and spectra from the event file. For the extraction of the lightcurves and the spectra, we chose a circular region for both the point source and the background. The size of the source region is set to the radius that includes 90% of the point spread function (PSF) at 1.5 keV obtained from the wavdetect algorithm, and for the background, we choose a source-free region within the same CCD chip. For the sources that are partially resolved such as in Figure 6, the extraction regions of the primary and the secondary source were carefully chosen to not overlap with one another using appropriate PSF fraction. In cases where the extraction regions of the primary and the secondary source overlap the common region between them was excluded to minimize the

¹ <https://xc.cfa.harvard.edu/caldb/downloads/index.html>

² <https://xc.cfa.harvard.edu/ciao/guides/>

source contamination (Skinner & Güdel 2014). This contamination was not significant in any of the cases.

The targets AK Sco, BD+30 549, BP PSc, HD 100546, R CrA, HBC 442, and HD 36982 are very faint and have been observed at different epochs. To obtain their spectrum with a better SNR, we co-added the spectra observed at different epochs, using the script “combine_spectra” (Table A1). This was performed only if the sources did not show variability at the different epochs. We checked the variability for these 7 sources by calculating the hardness ratio (HR) at different epochs using Equation (1). More details with respect to HR are provided in Section 3.1. The sample size in our work is quite large (44 X-ray emitting sources) compared to the previous studies. The X-ray parameters of 37 out of 44 HAeBe stars in our sample have previously been studied in the literature. Further, we found new X-ray detections for 7 HAeBe stars (See Table A1). In order to maintain homogeneity with respect to the data analysis, we re-analyzed the X-ray parameters for all the sources in our sample. The X-ray parameters obtained from our analysis agree well with the literature.

3.1 Temporal Analysis: X-ray Lightcurves

The 0.3 – 8 keV X-ray lightcurves are extracted for the sources with multiple observations. Only the lightcurves with good time resolution and statistics are used for the scientific analysis. We binned the lightcurves of all the detected sources to a fixed bin time. They are binned carefully to not contain any empty bins. The bin time used for the lightcurve of each source is mentioned in Figures D1 and D2. The HEASARC ftool “1cstats” is used to measure the “rms fractional variation” to check the variability of the lightcurve. The HR for all the X-ray emitting sources in the energy range 0.3 – 1 keV (S) and 1 – 8 keV (H) was calculated using equation (1).

$$HR = \frac{H - S}{H + S} \quad (1)$$

The following 9 sources, V892 Tau, HD 97300, TY CrA, HD 37062, V372 Ori, V380 Ori, HR 5999, HD 36939 and [DLM2010] EC 95 show flare-like features (Giardino et al. 2004; Hamaguchi et al. 2005). We observe a rapid rise in the count rate of these sources. To confirm this we calculated the HRs and observed a clear hardening. The HR of these stars increases with the increase in the count rate which is not observed for stars without variable/flaring lightcurves. The sources HD 97300 and EC 95 are observed only once while the rest of the 7 sources have multiple observations obtained over different epochs. HR 5999 has 7 multi-epoch observations and it is resolved only in the Obs ID: 8901, where HR 5999 was the prime target of the observation. HR 5999 A is very faint in X-rays, so its lightcurve could not be extracted. Similarly, the star V892 Tau has 2 multi-epoch observations and is resolved only in Obs ID: 3364. The lightcurves showing flaring/variability are presented in Appendix D. More details on the lightcurves are discussed in detail in Section 5.1.

3.2 Spectral Analysis: The X-ray Spectra

The X-ray spectra of HAeBe stars were extracted using the CIAO tool “specextract”. The Spectrum of each source was binned to a minimum of 5 or more counts/bin. The grouping was chosen based on the quality of the spectrum (i.e., the total number of counts). The sources having total counts < 100 are binned to contain a minimum of 5 counts/bin. For X-ray sources that have the total number of counts ≥ 100 , we binned the spectrum to contain a minimum of 15 counts/bin.

The spectral fitting was performed using the tool XSPEC version 12.11.1d (Arnaud 1996) available with HEASOFT (version 6.30). We used the plasma emission model “APEC” (Smith et al. 2001) along with “TBABS” for absorption correction. The solar abundances were set to values from Grevesse & Sauval (1998) for the plasma model and Wilms et al. (2000) for the absorption model. We tried fitting the spectrum with single temperature (1T) and two temperature (2T) models, considering four different model combinations on each spectrum i.e., 1T and 2T models with fixed or variable absorption column (N_H) from interstellar dust and the circumstellar material. For fits with fixed absorption, the N_H of the “TBABS” component was set to the values derived from the A_V , using the following equation taken from Bohlin et al. (1978),

$$\frac{N_H}{E(B - V)} = 5.8 \times 10^{21} \text{ cm}^{-2} \text{ mag}^{-1} \quad (2)$$

Since our work deals with HAeBe stars, we calculated the N_H considering an extinction factor $R_V=5$. A larger R_V is used as the circumstellar disk of HAeBe stars is dominated by grains larger in size than the average dust grain in the diffuse interstellar medium (Hernández et al. 2004; Manoj et al. 2006). The column density of the close companions is assumed to be equal to that of the HAeBe stars (Stelzer et al. 2006). Global metal abundances were fixed to 0.3 times the solar value (see, Imanishi et al. 2003; Feigelson et al. 2002, for details). For each source, the initial kT and the emission measure (EM) values for model fitting were taken from the literature.

To obtain the values of unabsorbed flux we use the convolution model “cf1ux” in the energy range 0.3 – 8 keV. We tried the model fitting with initial values of model parameters from the literature for four different model combinations (fixed and free N_H for 1T and 2T APEC models) for each source and adopted the fit with the minimum χ^2 . For χ^2 statistics the fit quality is determined by null-hypothesis probability (P_{NULL}). We evaluated the quality of the fit based on the P_{NULL} to check how well the spectrum is described by the model and accept only those spectral fits whose $P_{NULL} > 5\%$. First, we try the spectral fitting with the 1T model by fixing N_H to a value obtained from equation 2. We consider this model as the best fit if $P_{NULL} > 5\%$, else 1T model with free N_H is considered. If none of the 1T models gives a best fit, then the 2T model with fixed N_H is considered. Finally, if none of the models provide the best fit then we use the 2T APEC model with free N_H . The above method described is used only for χ^2 statistics which works best only for the bright sources (>100 counts) i.e., in our case, the stellar spectrum with at least 15 counts/bin, as this follows a Gaussian distribution (Bevington & Robinson 2003). The faint sources (<100 counts), i.e., stellar spectrum with less than 10 counts/bin are best explained by a simple Poissonian distribution. Here we used cash statistics (c-statistics) as the test statistic for such data. The quality of the fit for the c-statistics is determined by the “goodness” command which plots a histogram of probability versus χ^2 . If the statistic of observed data exceeds 90% of the simulated statistic values, then the model is rejected at 90% confidence³. The unabsorbed X-ray flux (F_X) is obtained from the model fitting and the unabsorbed X-ray luminosity (L_X) for all the sources is calculated using the formula,

$$L_X = 4\pi d^2 F_X \quad (3)$$

where d is the distance to the source. All the X-ray parameters in the model were obtained with a 90 percent confidence range. The

³ <https://heasarc.gsfc.nasa.gov/docs/xanadu/xspec/XspecManual.pdf>

X-ray parameters of the sources obtained by the above-mentioned methods agree well with previous studies (Stelzer et al. 2006, 2009a; Hamidouche et al. 2008).

The spectrum of sources MWC 297 A, MWC 297 B, HR 5999 A, T CrA and R Mon having very few counts (≤ 10 counts) could not be fit with a model. We obtained the count rate of these sources using the CIAO tool “apratex”. The L_X of these sources was then obtained using “PIMMS”, assuming an optically thin plasma of 10 MK (~ 1 keV), abundance of ~ 0.3 and the N_H derived from the A_V . The same procedure was used to estimate the upper limits of the L_X for the non-detected sources. The L_X of the source R CrA (counts > 100) was also obtained using PIMMS as the model parameters could not be constrained. Table B1 gives the X-ray parameters of stars fit with 1T and 2T APEC models for HAeBe sources and their companions. Table B2 gives the parameters for the sources that could not be detected in X-rays by *Chandra*.

4 RESULTS

Among our sample of 62 HAeBe stars, 44 of them show X-ray emission. *Chandra* has resolved 11 HAeBe stars among the 44, where the resolved companion is at a position $> 1''$. Of the 11 resolved systems, there are 5 stars with sub-arcsec companions. Apart from the resolved systems, there are 14 HAeBe stars with unresolved sub-arcsec companions i.e., companion stars within $1''$ of the primary which *Chandra* could not resolve. So, in total there are 19 out of 44 unresolved sub-arcsec multiple-star systems where i.) the primary and the secondary are HAeBe stars (e.g., AK Sco, V892 Tau), ii.) the primary and secondary are HAeBe stars with a TTS companion (e.g., R CrA, V380 Ori), and iii.) the primary is a HAeBe star and its companions are TTSs (e.g., TY Cra, HD 97300). In this paper, the group of 19 stars is identified as non-single stars. We evaluated a sub-arcsec companion (stars with separation $< 1''$) fraction of 43.1% for the stars detected in X-rays in this paper. 25 out of 44 stars (56.8%) are either confirmed to have no stellar companions or have any evidence of the presence of a companion as of yet (we name this group as ‘single stars’). The details of the companion status of the HAeBe stars in our sample are given in Table C1.

The X-ray parameters (kT , L_X and N_H) of HAeBe stars in our sample obtained from X-ray spectral analysis are tabulated in Table B1. To understand the origin of the X-ray emission in HAeBe stars, we compare their X-ray parameters with other stellar parameters such as bolometric luminosity, temperature, infrared excess, and accretion. Further, we compare the properties of HAeBe stars with those of TTSs. The parameters of TTSs in the ONC are obtained from the COUP analysis (Getman et al. 2005), as discussed in Section 2.2.

4.1 Estimation of L_X/L_{bol} of HAeBe stars and their variation with spectral type

The variation of X-ray luminosity with bolometric luminosity (L_{bol}) for HAeBe stars (our sample) and the TTSs from the COUP sample is shown in Figure 1. We compute the bolometric luminosity of HAeBe stars as follows. The observed apparent magnitude (m_V) is corrected for extinction (A_V) and using the distance modulus relation we calculated the absolute magnitude (M_V). The distances to the sources used for the calculation are mentioned in Table A1. The m_V for HAeBe stars were obtained from Manoj et al. (2006), Mathew et al. (2018), and Vioque et al. (2018). From M_V we estimated the bolometric magnitude (M_{bol}) using the values of bolometric correction corresponding to each spectral type, from the table listed in Pecaut &

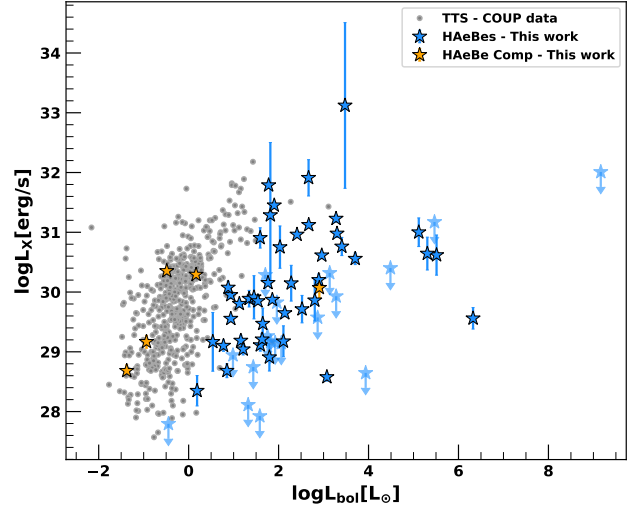


Figure 1. X-ray luminosity (L_X) against bolometric luminosity (L_{bol}). Grey dots – TTSs (ONC), blue stars – HAeBe stars(our sample), orange stars – close companions to HAeBe stars (our sample), faint blue stars – upper limits (X-ray dark sources).

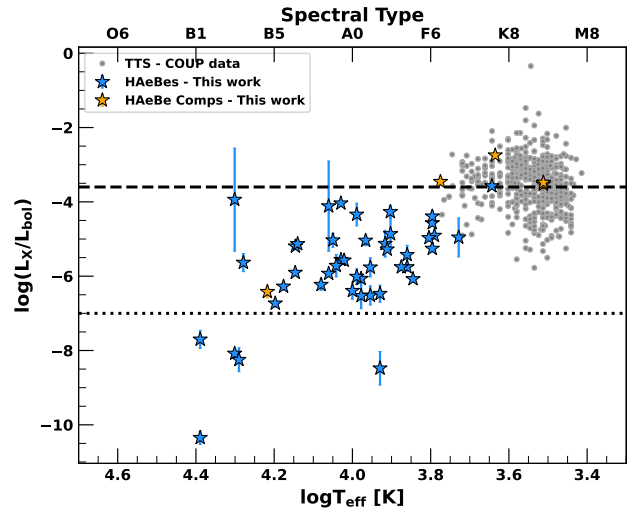


Figure 2. Variation of fractional X-ray luminosity against the temperature and spectral type. The dashed line denotes the mean L_X/L_{bol} of TTSs ($10^{-3.6}$) and the dotted line that of main-sequence OB type stars (10^{-7}).

Mamajek (2013). We then calculate the bolometric luminosity (L_{bol}) of the HAeBe stars using the equation below,

$$\log\left(\frac{L_{bol}}{L_{\odot}}\right) = \left(\frac{M_{bol\odot} - M_{bol}}{2.5}\right) \quad (4)$$

where, the bolometric magnitude of the Sun $M_{bol,\odot} = 4.75$. The bolometric luminosity and the unabsorbed X-ray luminosity for the TTSs are obtained from Getman et al. (2005).

From Figure 1, we see that the L_{bol} - L_X distribution of HAeBe stars and TTSs follow a similar trend, with TTSs being more steeper. The X-ray luminosities of both the stellar groups are slightly different, ranging from around 10^{28} to 10^{33} erg s^{-1} for HAeBe stars and 10^{27} to 10^{32} erg s^{-1} for TTSs. We see there is a necessity to normalize the L_X , as this gives us an estimate of how bright or faint the HAeBe

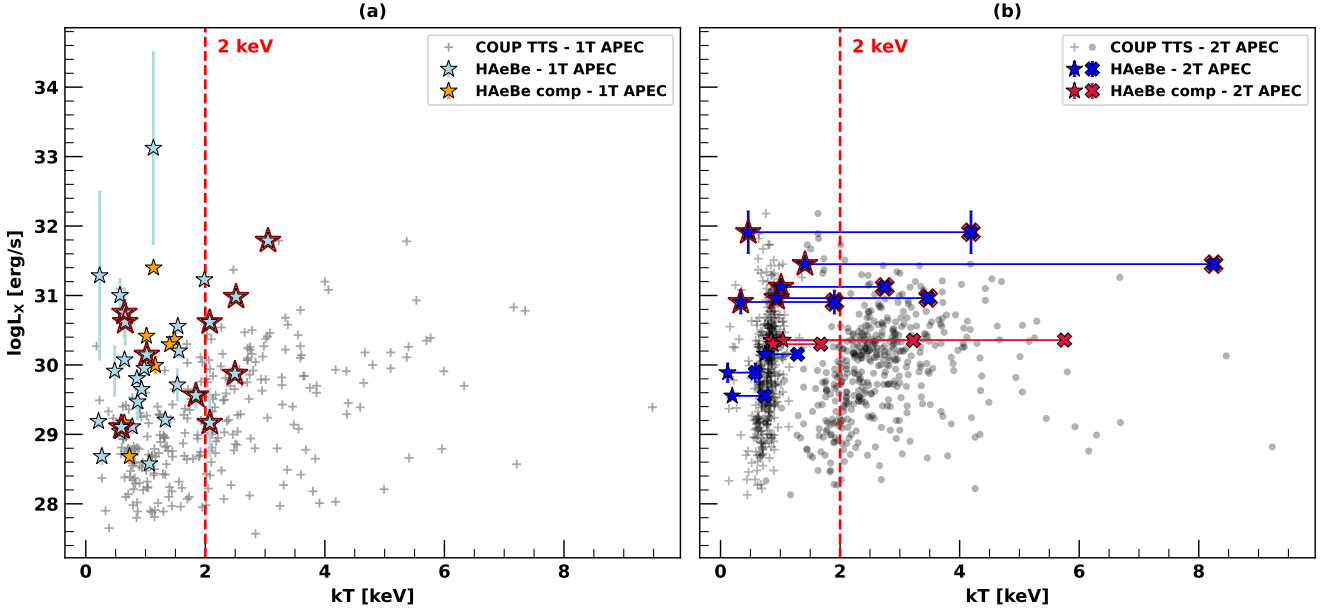


Figure 3. (a). kT vs L_X plot for stars fitted with 1T APEC model. The light grey “+” symbol denotes TTSs fitted with 1T model and the light blue “filled star” symbol denotes HAeBe stars fitted with 1T APEC model. The orange “filled star” symbol denotes the resolved companions of HAeBe stars, (b). kT vs L_X plot for stars fitted with 2T APEC model. The grey “+” and “o” symbols denote $kT1$ and $kT2$ of TTSs, respectively whereas dark blue “filled star” and “filled cross” symbols denote $kT1$ and $kT2$ of HAeBe stars, respectively. The red “filled star” and “filled cross” symbols denote $kT1$ and $kT2$ of the resolved companions of the HAeBe stars. The blue and red lines connecting these symbols represent the plasma temperatures of their respective stars; The stars outlined in red represent the HAeBe stars with unresolved companions. The red dashed line is marked at 2 keV denoting the plasma temperature within which single HAeBe stars are found.

stars are in X-rays compared to TTSs. Hence, we now consider the plot of L_X/L_{bol} against effective temperature/spectral type (Figure 2). The effective temperature (T_{eff}) for HAeBe stars were obtained from Manoj et al. (2006), Hamidouche et al. (2008) and Vioque et al. (2018). For TTSs, we obtained the T_{eff} by cross-matching the final list of TTSs (see, Section 2.2) with Da Rio et al. (2012). The T_{eff} was converted to spectral type using the table listed in Pecaut & Mamajek (2013).

We see from Figure 1 that, although the L_X of HAeBe stars and TTSs are not substantially different, their L_X/L_{bol} appear to greatly differ. It is apparent from Figure 2 that the L_X/L_{bol} of HAeBe stars is lower by about 3 to 4 orders of magnitude when compared to that of TTSs. In order to provide a visual comparison in Figure 2, we have marked the average L_X/L_{bol} of TTSs ($10^{-3.6}$) (Preibisch et al. 2005) with a horizontal dashed line and that of MS OB stars (10^{-7}) (Nazé et al. 2011) with a horizontal dotted line. The L_X/L_{bol} of most of the HAeBe stars in our sample (86%) fall in between the mean value of TTSs and OB stars. The L_X/L_{bol} of HAeBe stars decrease with increasing T_{eff} , i.e., massive HAeBe stars emit lesser X-ray flux. We do not observe such a trend for TTSs.

4.2 Variation of L_X with kT

The X-ray spectra of PMS stars could fit well with a 1T or 2T absorbed thermal plasma model (Getman et al. 2005). The plasma temperatures (kT) for the HAeBe stars in our sample were estimated as discussed in Section 3.2 and it agrees well with the literature (Hamaguchi et al. 2005; Stelzer et al. 2006, 2009a). While the coronal temperature is unlikely to be isothermal or be approximated by 1T or 2T models, we still follow this approach as our aim is to homogeneously characterize the plasma temperatures of HAeBe stars

in our sample. The plasma temperatures obtained from the model fitting of the X-ray spectrum can be considered as a characteristic temperature (Peres et al. 2004; Preibisch et al. 2005) and hence we use this parameter to see its variation with L_X . Figure 3 shows the kT versus L_X for HAeBe stars (our sample) and TTSs (COUP sample). Figure 3(a) represents the HAeBe stars and TTSs that fit with the 1T APEC model and Figure 3(b) represents the HAeBe stars and TTSs that fit with the 2T APEC model. In the case of TTSs fitted with 1T model (Figure 3a), the plasma temperature of a majority of them is on the hotter side i.e., kT ranging from 0.18 to 9.5 keV. However, in the case of TTSs with 2T model fits (Figure 3b), we observe a cool component ($kT1$) ranging from 0.14 to 1.37 keV and a hot component ($kT2$) ranging from 0.72 to 9.23 keV (Preibisch et al. 2005). The cool component seems to be constant at ~ 10 MK ($kT \sim 1$ keV), while the hot component seems to increase with increasing L_X . An increase in kT with increasing L_X is also observed for the TTSs with 1T fit (Figure 3a). HAeBe stars with 1T fit which have no known companions have plasma temperatures in the range 0.21 to 1.98 keV, and HAeBe stars with sub-arcsec companions (stars outlined in red in Figure 3a) have plasma temperatures in the range from 0.65 to 3.05 keV. In the case of HAeBe stars with 2T fit having no known companions, the plasma temperature $kT1$ ranges from 0.12 to 0.20 keV and $kT2$ from 0.58 to 0.74 keV, whereas for HAeBe stars with sub-arcsec companions (stars outlined in red in Figure 3b), the plasma temperature $kT1$ ranges from 0.34 to 1.41 keV and $kT2$ from 1.29 to 8.25 keV. The sub-arcsec companions to HAeBe stars vary from being low mass to similar mass stars (Table C1). We see hotter plasma temperatures ($kT > 2$ keV) for TTSs than that for single HAeBe stars, which are relatively cooler i.e., $kT \leq 2$ keV (See Table B1). The plasma temperatures of HAeBe stars with sub-arcsec companions are hotter ($kT > 2$ keV), similar to TTSs. About 50% of the non-single HAeBe stars

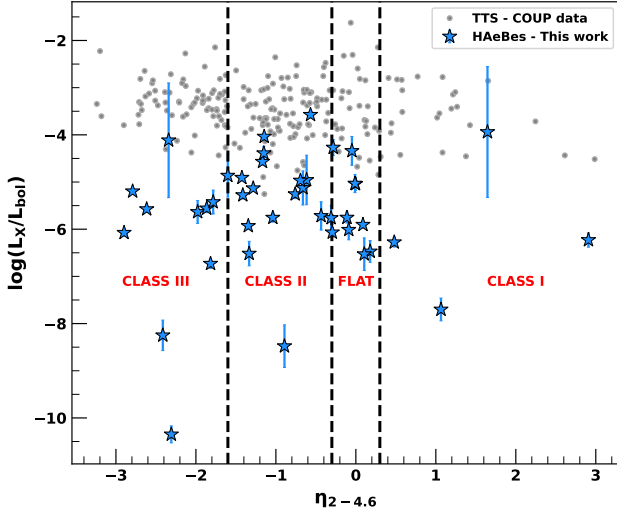


Figure 4. IR Spectral Index against L_X/L_{bol} showing the classification scheme by Greene et al. (1994). Class I ($\eta \geq 0.3$), Flat ($-0.3 \leq \eta < 0.3$), Class II ($-1.6 \leq \eta < -0.3$), Class III ($\eta \leq -1.6$).

fit with the 1T model and 80% non-single H AeBe stars fit with the 2T model have $kT > 2$ keV.

4.3 Estimation of IR spectral index and its variation with L_X/L_{bol}

It is understood from the infrared studies of H AeBe stars (Manoj et al. 2006; Chen et al. 2016) that the IR flux excess is due to the presence of dust in their circumstellar disk. Lada (1987) showed that the IR spectral index is one of the important criteria used to identify the presence of the disk in YSOs. In this work, we used the IR spectral index $\eta_{(2-4.6)}$ as an indicator of IR excess. A classification scheme for YSOs was quantified by Greene et al. (1994) using the slope of the SEDs in the IR region. The YSOs are distributed into 4 classes, described as Class I ($\eta \geq 0.3$), Flat ($-0.3 \leq \eta < 0.3$), Class II ($-1.6 \leq \eta < -0.3$), Class III ($\eta \leq -1.6$). We obtained the spectral indices in the K_S -W2 IR band for our sample using the method described in Manoj et al. (2011) and Arun et al. (2019). The spectral index was calculated using the following equation,

$$\eta_{(\lambda_1-\lambda_2)} = \frac{\log\left(\frac{\lambda_2 F_{\lambda_2}}{\lambda_1 F_{\lambda_1}}\right)}{\log\left(\frac{\lambda_2}{\lambda_1}\right)} \quad (5)$$

where, λ_1, λ_2 are the two wavelengths considered, and $F_{\lambda_1}, F_{\lambda_2}$ are the flux values at λ_1, λ_2 .

Figure 4 shows the plot of $\eta_{(2-4.6)}$, an indicator of infrared excess between K_S and W2 bands, against the L_X/L_{bol} for H AeBe stars and TTSs. The excess NIR emission in H AeBe stars is from their inner disk (Dullemond & Dominik 2004a,b, 2005). Most of the stars in our sample fall under Class II and flat group, which indicates that a majority of the stars in our sample possess a circumstellar disk. We see in Figure 4 that similar to TTSs, H AeBe stars do not follow a relation between L_X/L_{bol} and $\eta_{(2-4.6)}$. We see that the L_X/L_{bol} of both samples does not seem to be affected by the presence or absence of the disk. Further, we need to investigate if the accretion of matter from the circumstellar disk to the star is responsible for the X-ray emission in H AeBe stars, which is evaluated in Section 4.4.

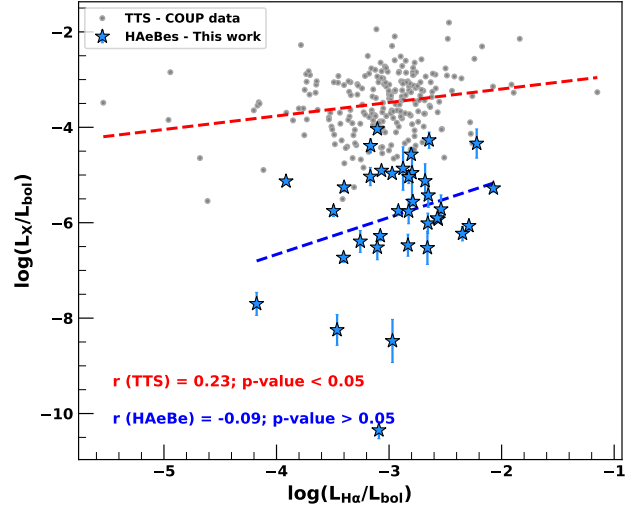


Figure 5. $L_{H\alpha}/L_{bol}$ of H AeBe stars (Blue star) and TTSs (grey dot) plotted against the L_X/L_{bol} . The Pearson's coefficient for H AeBe stars and TTSs is $r = -0.09$; p -value = .00051 and $r = 0.23$; p -value = 0.60167, respectively.

4.4 Estimation of $L_{H\alpha}/L_{bol}$ and its variation with L_X/L_{bol}

We know that TTSs accumulate mass through the magnetospheric accretion process. According to this paradigm, the magnetic field lines from the star truncate the disk, and the material from the disk is transferred onto the star. When the in-falling material shocks the photosphere, X-rays are emitted (Calvet & Gullbring 1998). It is known that the $H\alpha$ emission line is a good tracer of accretion in PMS stars. Hence, to investigate if the accretion mechanism in H AeBe stars is contributing to the emission of X-rays, we calculate the $H\alpha$ luminosity ($L_{H\alpha}$) and plot the $L_{H\alpha}/L_{bol}$ against L_X/L_{bol} (Figure 5). We calculated the $H\alpha$ flux using the method described in Mathew et al. (2018). They used the extinction corrected R-band flux density as a proxy for the continuum flux density underlying the $H\alpha$ line, from which the continuum $H\alpha$ flux ($F_{v,cont(H\alpha)}$) is obtained using the equation 6,

$$F_{v,cont(H\alpha)} = F_{v,0} \times 10^{\left(\frac{-R_0}{2.5}\right)} \quad (6)$$

where $F_{v,0} = 3.08 \times 10^{-23} \text{ W m}^{-2} \text{ Hz}^{-1}$ and R_0 is extinction corrected magnitude. The extinction in R-band (A_R) was estimated from A_V using the extinction curve of McClure (2009). From the $F_{v,cont(H\alpha)}$, we estimated the $H\alpha$ line flux using $F_{\lambda,line(H\alpha)} = F_{v,cont(H\alpha)} \times EW(H\alpha)$. The absorption corrected equivalent width ($EW(H\alpha)$) for H AeBe stars was obtained from the literature (Manoj et al. 2006; Fairlamb et al. 2017; Vioque et al. 2018; Wichittanakom et al. 2020). The $H\alpha$ luminosity ($L_{H\alpha}$) is then calculated using the standard flux-luminosity relation, similar to Equation 3. Figure 5 shows the plot of $L_{H\alpha}/L_{bol}$ against L_X/L_{bol} for both H AeBe stars and TTSs. We perform Pearson's correlation test to check for a linear relation between X-ray emission and the accretion processes. For TTSs, we obtain Pearson's co-efficient $r = 0.23$ with a p -value = 0.0005 and for H AeBe stars we obtain $r = -0.09$ with a p -value = 0.6017 at a significance (α) level of 0.05. These values suggest that, for TTSs and H AeBe stars, we do not observe any correlation between $L_{H\alpha}/L_{bol}$ and L_X/L_{bol} . This strongly suggests that the accretion process is not a major contributor to the production of X-rays in TTSs and H AeBe stars.

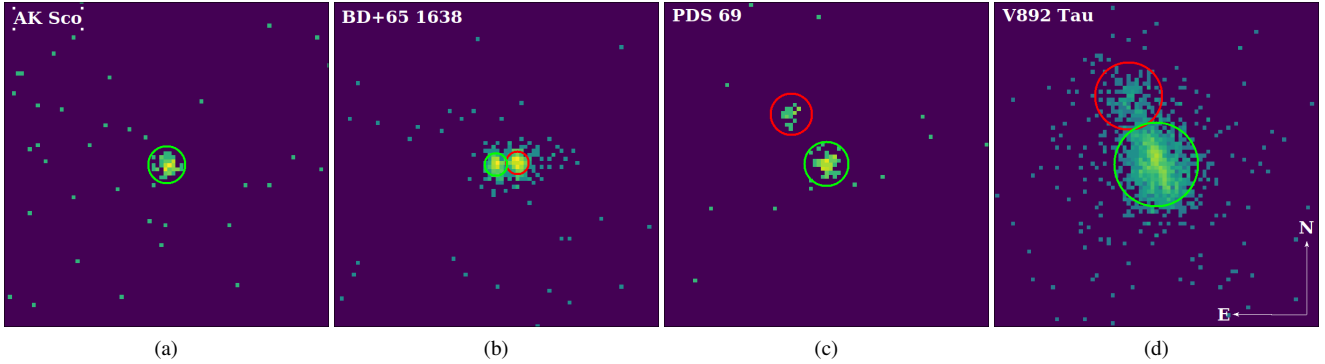


Figure 6. 20" x 20" ACIS – CCD images of the HAeBe stars having equal mass companions (possible HAeBe stars). The images are binned to a pixel size of 0.25". the green circle denotes the photon extraction region of the primary star and the red circle denotes the photon extraction region of the secondary star. For the sources, BD+65 1638 A & B and V892 Tau B, the radius of extraction regions was set to a PSF fraction of 0.84.

5 DISCUSSION

Quite a few mechanisms have been proposed to explain the X-ray emission from HAeBe stars, with the prominent ones being due to the contribution from a low-mass (undetected) companion in the close proximity of the HAeBe star (Stelzer et al. 2006, 2009a), colliding winds producing X-ray emission (similar to what is seen in massive OB-type stars: Zinnecker & Preibisch 1994; Damiani et al. 1994), presence of a shear-powered dynamo in late-type HAeBe stars (Tout & Pringle 1995), the magnetically confined wind shock model (MCWS) (Swartz et al. 2005; Telleschi et al. 2007b), and magnetospheric accretion shock model (Calvet & Gullbring 1998). From the results obtained in this paper, we propose that the X-ray emission from HAeBe stars has a different origin than TTSSs. In the following sub-sections, we rule out the possibility of the presence of an unseen low-mass companion as solely the origin of X-rays and discuss the possible X-ray mechanisms that contribute to the emission of X-rays in HAeBe stars.

5.1 Role of binaries

In this section, we discuss the details of the various types of companions mentioned in Section 4 and present three observational details that support intrinsic X-ray emission from HAeBe stars.

(i) **Planetary studies – The presence of planetary companions around the X-ray emitting HAeBe stars:** Some stars in our sample were studied individually using high-resolution instruments and adaptive optics. There were no strong signatures of stellar companions, though planetary companions were discovered. Among the 25 single HAeBe stars, 7 such systems are present. For example, the HAe star AB Aurigae has been studied extensively (e.g., Boccaletti et al. 2020; Currie et al. 2022; Zhou et al. 2022). Fukagawa et al. (2004) studied AB Aur in the NIR region using the Coronagraphic Imager Adaptive Optics systems on the Subaru telescope, in which spiral features within the circumstellar matter were discovered. Tang et al. (2012) suggested the presence of an unseen companion to AB Aur at 30 AU as the probable reason for the observed spiral patterns in the disk. A follow-up paper by Tang et al. (2017) identified two spirals in high-resolution ALMA $^{12}\text{CO } J = 2 - 1$ emission observations and suggested that the spiral arms are due to several protoplanets present at 60 – 80 AU ($0''.4 - 0''.6$ separation) and another companion at 30 AU ($0''.16 - 0''.18$ separation). Boccaletti et al. (2020) presented VLT/SPHERE observations of AB Aur and

suggested that the two spirals observed in the system are due to the protoplanetary candidates at around 30 AU ($\sim 14M_{\text{Jup}}$) and 110 AU ($\sim 3M_{\text{Jup}}$) from the center of the star. Similarly, the Herbig Be star HD 100546 was studied by Pérez et al. (2020) using the Atacama Large Millimeter/submillimeter Array. They found evidence for the signatures of 2 protoplanets ($\sim 3.1M_{\text{Jup}}$ & $8.5M_{\text{Jup}}$; Fedele et al. 2021) and ruled out the possibility of stellar companions by their sparse-aperture masking data. HD 163296 was studied by Kirwan et al. (2022) using spectro-images and position velocity diagrams extracted from the MUSE data cube. They ruled out the presence of any stellar companions within 1 AU – 35 AU and suggested the presence of either a brown dwarf or a massive planet. The details of other stars supporting the evidence of protoplanetary candidates in their inner disk regions are tabulated in Table C1 with references. These studies strongly rule out the presence of a stellar companion. Also, the type of X-ray emission observed from the group of stars identified as single stars is towards the cooler side ($kT \leq 2$ keV), as discussed in Section 4.2.

(ii) **Similar mass companions to the X-ray emitting HAeBe stars:** In our sample of stars, there are 4 stars that possess a similar mass/HAeBe star as companions, with no other low-mass companion reported (see, Table C1). Figure 6 shows the 20" x 20" ACIS images binned to a pixel size of 0.25" of the HAeBe stars having companions that are possibly HAeBe stars. The details of these 4 stars are discussed below.

AK Sco: AK Sco (HD 152404) is a spectroscopic binary (SB2; Andersen et al. 1989) system consisting of two equal-mass (total $M_{\star} = 2.49M_{\odot}$) F5-type stars, with a period of 13.6 days and a large eccentricity ($e = 0.47$). The distance of separation between the two stellar components is ~ 0.16 AU and they come as close as $11R_{\star}$ at the periastron. From the high-resolution studies (Esposito et al. 2020) there has been no detection of another low-mass star in this system. The system has been observed thrice using CXO. Due to its very low quality, we combined the data to obtain a good-quality spectrum (see, Section 3.2). The details of the X-ray parameters are given in Table B1. We see a very cool plasma temperature ($kT \sim 0.6$ keV) and no variability in the lightcurve.

BD+65 1638: BD+65 1638 is one of the three massive HBe stars in the reflection nebula NGC 7129. It has a spectral type of B2-B3 (Racine 1968; Matthews et al. 2003). Dahm & Hillenbrand (2015) first suggested for the star to be spectroscopic binary. From the source's L_{\star} and T_{eff} , the star is placed very close to the birth-line of a $6M_{\odot}$ object (Matthews et al. 2003). In *Chandra* ACIS data the star is

resolved into 2 X-ray bright sources with a separation of $\sim 1.3''$ (Figure 6(b)). This system is one of the bright HBe stars in our sample. The X-ray spectra of both the stars fit well with 1T APEC plasma model with plasma temperature $kT = 1.98$ keV for BD+65 1638 A and $kT = 1.13$ keV for BD+65 1638 B. The plasma temperature of component A is slightly higher than that of component B. The L_X for both the stars is within the range for B-type stars. We do not observe any variability/flaring in the lightcurve of both the sources. The stellar system seems to be unusually in a quiescent state, as the star has just emerged out of the gaseous envelope.

PDS 69: PDS 69/H4636 is associated with the reflection nebula NGC 5367. This is a double-star consisting of two B-type stars of spectral types B7 (PDS 69 A) and B4 (PDS 69 B). The system is a wide binary at an angular separation of $\sim 3.7''$. Both the stars show IR excess and the northern component i.e., PDS 69 B shows H α in emission (Williams et al. 1977; Maheswar et al. 2002). From their positions in the CMD, PDS 69 A and PDS 69 B appear to have masses of about 4.5 and 8 M_\odot , respectively (Williams et al. 1977). The wide binary is well resolved in X-rays (*Chandra* data). The ACIS CCD image is shown in figure 6 (c). The X-ray spectrum is fitted with 1T APEC model for PDS 69 A, with plasma temperature $kT = 1.56$ keV and $L_X = 1.58 \times 10^{30}$ erg s^{-1} . As PDS 69 B is very faint, we used PIMMS to obtain the $L_X = 1.17 \times 10^{30}$ erg s^{-1} . The X-ray lightcurve of PDS 69 A does not show any signs of variability/flaring or any hard X-ray emission. This double-star system is one example of two resolved HAeBe stars emitting X-rays with no known third unresolved companion.

V892 Tau: V892 Tau (Elias 3-1) is a late HAeBe star in the Taurus-Aurigae star-forming region (Smith et al. 2005). It has a spectral type ranging from B9 to A6 (Alonso-Albi et al. 2009; van der Marel et al. 2016). It is a triple star system, consisting of a central binary of equal mass ($\sim 6M_\odot$) separated by ~ 7 AU and an M5-type TTS at ~ 500 AU ($\sim 4''$) from the central binary (Long et al. 2021). We denote the central binary as V892 Tau A and the M-type companion as V892 Tau B. The star has been studied previously in X-rays by Stelzer et al. (2006) and Giardino et al. (2004). We analyzed the *Chandra* data available for 2 epochs. The system could be resolved from the M-type companion only in one of the observations (Obs ID: 3364) as the coordinates of V892 Tau was near the aim-point of the observation (Figure 6 (d)). In our analysis, the *Chandra* X-ray spectrum was fit with a 2T APEC model ($kT_1 = 1$ keV & $kT_2 = 2$ keV). A flare is observed in the ~ 18 ks X-ray lightcurve, from the region of the central binary, and no variability/flare in the position of the M-type low-mass companion was seen. We also analyzed the observation (Obs ID: 2522) where the source was not resolved, and the X-ray lightcurve showed some variability with a count rate similar to that of the central binary in Obs ID: 3364 (see, Appendix D1). The origin of the flare seems to be coming from the two nearly equal mass HAeBe stars (Giardino et al. 2004). Similar characteristics are observed in V372 Ori, which is a spectroscopic binary with an A-type PMS companion. However, many details are not known about this star and it is a good candidate for future studies.

(iii) **HAeBe stars which present flaring/variability:** Appendix D shows the lightcurves of the 9 HAeBe stars stellar systems unresolved with *Chandra*. Of the 44 stars detected in X-rays, we see X-ray lightcurve variability (short term and long term) and flaring in 9 stars (see, Section 3.1; Appendix D). 6 of these have low-mass companions (TY CrA, V380 Ori, HR 5999, HD 97300, [DLM2010] EC 95 and HD 37062), 2 have a similar mass companion (V892 Tau, V372 Ori) and 1 (HD 36939) have no companions as of now. X-ray flares in low-mass PMS like TTSs are very common and are characterized by rapid enhancement in the count rate which is followed by slow

decay Caramazza et al. (2007). Low-mass PMS stars show thermal emission with a $kT \sim 1 - 8$ keV and a strong variability with occasional rapid flares consistent with the scenario of enhanced solar-type activity, attributable to magnetic dynamo processes (Imanishi et al. 2003; Preibisch et al. 2005). Such characteristics are observed in the HAeBe stars with low-mass companions. TY CrA shows a large flare lasting for more than 10ks. While V380 Ori, HR 5999, HD 97300, and HD 37062 also show flare-like properties, their observation does not contain the details of the whole flare (rise and decay). [DLM2010] EC 95, a proto-Herbig star (Dzib et al. 2010) shows short term variability. The plasma temperature of these stars is very high, on the hotter side ranging from $kT = 2.75 - 8.25$ keV (Figure 3a & b). V892 Tau, and V372 Ori are the only two HAeBe stars known to show flaring activity, with a similar flare shape (Figure D1). This is unusual for HAeBe stars as they do not possess convective layers like low-mass stars. The plasma temperature of V892 Tau is very close to what we see for single HAeBe stars in this paper ($kT \sim 2$ keV; Section 4.2). V372 Ori has a plasma temperature ($kT_1 = 0.94$ keV; $kT_2 = 3.75$ keV) and flare characteristics as seen in low-mass stars. It is identified as a spectroscopic binary (Abt et al. 1991) consisting of a B9.5+A0 stellar system. The lightcurve of HD 36939 has a very low count-rate (~ 0.002 cts/s) compared to other stars, but we see variability in the count-rate in only one (Obs ID: 4395) of the 14 observations (spanned over a period of 13 years). More high-resolution studies are required to understand the properties of these stellar systems.

The above-mentioned are details of types of sub-arcsec companions to HAeBe stars in our sample (i.e., planetary, similar mass and low-mass companions). The temperature structure of single HAeBe stars and HAeBe stars with companions seems to be different. We see that single HAeBe have cooler plasma temperatures compared to the non-single stars. From the discussion, we can see that in HAeBe stars, X-ray emission is not confined to one mechanism. In Section 5.3, we discuss the possible emission mechanisms that can explain the origin of X-ray emission in HAeBe stars.

5.2 Magnetic fields in Herbig Ae/Be stars

Magnetic field has been detected in very few HAeBe stars. Hubrig et al. (2009) studied 21 HAeBe stars using FORS1 mounted on the 8m Kueyen telescope of the VLT. They detected magnetic fields for all of the sources in their sample with a confidence level of $\sim 1\sigma$. Among the 21 HAeBe stars, 10 were detected with a significance level $> 3\sigma$. The magnetic fields varied from less than 10 G to ~ 500 G. On cross-matching the X-ray emitting stars in our sample with Hubrig et al. (2009), we find 11 stars (HD 100453, HD 100546, HD 135344B, HD 144432, HD 144668, HD 150193, AK Sco, HD 163296, HD 169142, HD 190073, HD 97300) to possess magnetic field (see, Table 3 Hubrig et al. 2009). Alecian et al. (2009) studied the multiple-star system V380 Ori using high-resolution spectropolarimeters ESPaDOs, installed on the 3.6 m CFHT, and Narval, installed on the 1.9 m TBL. They measured a magnetic field strength of ~ 500 G for the primary. No magnetic field was detected for the secondary component. Hubrig et al. (2011) studied HD 31648 using high-resolution polarimetric spectra obtained with SOFIN spectrograph installed at Nordic Optical Telescope. A variable longitudinal magnetic field of the order of a few hundred Gauss up to one kG (-952 ± 177 G) was measured. Another study by Hubrig et al. (2013), measured magnetic fields on 6 HAeBe stars using the HARPS in spectropolarimeter mode. They measured a weak magnetic field of ~ 65 G for HD 104237. Järvinen et al. (2015), was able to

measure the magnetic field of the primary (~ 13 G) and the secondary (~ 129 G) of the HD 104237 system using HARPS spectrograph. The primary is a HAe star and the secondary is a TTS (Table C1). Petit et al. (2008) detected a magnetic field strength of -240 ± 70 G was detected for HD 36982. This was further confirmed by Alecian et al. (2013) with moderate detection. We see that the Herbig Ae/Be stars possess much weaker magnetic fields than their lower mass counterpart T Tauri stars which have magnetic fields in kG (Järvinen et al. 2019b). The 15 HAeBe stars mentioned in the above discussion emit X-rays whose origin is intimately linked to the presence of the magnetic field. Of these 15 stars, 11 are single HAeBe stars and 4 are non-single HAeBe stars. We find that from our sample of 25 single HAeBe stars, 11 are confirmed to have magnetic fields. Apart from these 11 confirmed magnetic field detections, magnetic fields were measured on 4 single HAeBe stars. However, only upper limits were obtained. For the remaining 10 single HAeBe stars magnetic field detections have not been studied. Among the 19 non-single HAeBe stars, 4 stars are confirmed to have magnetic field detections. Upper limits were measured for 3 non-single HAeBe stars. The magnetic fields of the remaining 12 non-single HAeBe stars have not yet been studied. Further studies on measuring the magnetic fields of X-ray-emitting HAeBe stars would provide more insights.

5.3 Possible X-ray emission mechanisms in HAeBe stars

Sun-like stars contain outer convection zones and the X-rays from the corona are linked to a solar-like dynamo. A similar mechanism is thought to be the origin of X-rays in TTSs (Preibisch et al. 2005; Telleschi et al. 2007a). Magnetospheric accretion and coronal X-ray are mainly the reason for X-ray emission in TTSs. Massive OB-type stars produce X-rays from radiation-driven instability shocks and magnetically confined wind shocks (Babel & Montmerle 1997b; Zhekov & Palla 2007; Montmerle 2007). Radiative wind models are also ruled as the temperatures of HAeBe stars are not hot enough for the winds to be generated. From the results obtained in this study, we see that the L_X with respect to the L_{bol} decreases towards earlier type stars (Figure 1 & 2), suggesting a decrease in the X-ray activity levels towards early-type stars. Wichittanakom et al. (2020) showed that the mass-accretion rates and accretion luminosity of HAeBe stars increase with the increase in mass. Our studies show that $L_{\text{H}\alpha}$, which is a good tracer of mass accretion rate, does not correlate with the L_X of HAeBe stars, strongly suggesting that in-falling material from the disk is not responsible for X-ray emission (Figure 5). Stelzer et al. (2006) and Stelzer et al. (2009a) suggest that X-ray emission in HAeBe stars could be attributed to hidden low mass companions, as the binarity rate of their sample was high and also the X-ray properties were very similar to that of other low-mass stars. In Section 5.1, we have documented high-resolution studies that confirm the presence of planetary companions rather than stellar companions in our HAeBe sample (Table C1). Similarly, for HAeBe stars with confirmed unresolved low mass companions, some of which are observed at multi-epochs, we observe long-term and short-term variability with flaring in their X-ray lightcurves. This result along with the soft/cool X-ray temperature of single HAeBe stars and similar mass HAeBe systems suggests that the X-ray emission in HAeBe stars may not be solely due to hidden TTSs but is intrinsic to the star itself. But, what could be the emission mechanism involved in the production of X-rays in HAeBe stars?

Telleschi et al. (2007b) and Günther & Schmitt (2009) studied the high-resolution X-ray spectra of HAeBe stars AB Aurigae, and HD 163296, respectively, which are obtained from the XMM-Newton Reflection Grating Spectrometers (RGS) and EPIC instru-

ments. These stars are confirmed to be single and not known to have any sub-arcsec companions from the high-resolution studies discussed in Section 5.1. The X-ray spectra of both stars are very soft with low photoelectric absorption (the spectrum falls off rapidly above 1 keV) pointing to a cool source. AB Aurigae has temperature components of $kT_1 = 0.21^{+0.03}_{-0.03}$ keV, $kT_2 = 0.6^{+0.03}_{-0.04}$ keV, and $L_X = 4 \times 10^{29}$ erg s^{-1} in the energy range 0.3 – 10.0 keV (Telleschi et al. 2007b). While, HD 163296 has temperature components $kT_1 = 0.21^{+0.03}_{-0.01}$ keV, $kT_2 = 0.51^{+0.1}_{-0.03}$ keV, $kT_3 = 2.7^{+1.5}_{-0.8}$ keV, and $L_X = 4.1 \times 10^{29}$ erg s^{-1} in the energy range 0.2 – 8.0 keV (Günther & Schmitt 2009). About 35% of the emission measure was found at 0.2 keV for AB Aurigae, whereas it is $\sim 60\%$ for HD 163296. Further, Günther et al. (2013) studied the *Chandra* data of the source HD 163296, using the same method as in Günther & Schmitt (2009) and obtained similar model parameters with $kT_1 = 0.19^{+0.23}_{-0.02}$ keV, $kT_2 = 0.60^{+0.05}_{-0.04}$ keV, $kT_3 = 2.0^{+1.0}_{-0.5}$ keV, and $L_X = 3.8 \times 10^{29}$ erg s^{-1} for Obs ID: 3733 and $kT_1 = 0.16^{+0.01}_{-0.01}$ keV, $kT_2 = 0.60^{+0.2}_{-0.02}$ keV, $kT_3 = 2.4^{+0.5}_{-0.3}$ keV and $L_X = 6.3 \times 10^{29}$ erg s^{-1} for Obs ID: 12359. These values within the error bars are consistent with our study. Telleschi et al. (2007b) and Günther & Schmitt (2009) analyzed the density-sensitive He-like line triplets of O VII, observed in the high-resolution spectra of AB Aurigae, and HD 163296. The flux ratio of the forbidden (f) to intercombination (i) lines (i.e., $\mathcal{R} = f/i$ ratio) at 22.1 Å, and 21.8 Å, respectively, point to the low-density regions (such as stellar coronae; $n_e < 10^{11}$ cm^{-3}) as the location for the production of majority the of X-ray emission. The lightcurve of AB Aurigae shows a period of ~ 42 hours which is consistent with the modulation period of Mg II and He I lines formed in the chromosphere. No such period was found in the lightcurve of HD 163296, but a short-term variability was observed. Both studies reject the accretion shock model and companion hypothesis. The accretion shock model is rejected based on the high f/i line ratios obtained from the triplets which suggest a low-density environment as the formation region of X-rays, whereas accretion shocks are generated in regions close to the stellar photosphere, in the high-density regions. HD 163296 drives a jet HH 409, which could be the reason for the excessive soft X-ray emission, while the ~ 2 keV component could be from the coronae. The above-mentioned characteristics observed in the high-resolution X-ray spectra of the HAeBe stars AB Aurigae, and HD 163296 clearly point to X-ray emission in the low-density regions such as coronae which supports the presence of magnetic fields in these stars. Based on the evidence discussed above, Telleschi et al. (2007b) and Günther & Schmitt (2009) suggested either a wind shock model or magnetically confined winds could be the mechanism responsible for the emission of X-rays.

From the above discussion on individual stars AB Aurigae, and HD 163296 and the magnetic field detections of the HAeBe stars in Section 5.2. It is plausible to say that the X-ray emission in HAeBe stars is due to the presence of magnetic fields. However, the origin of the magnetic field remains unknown. In the study by Hubrig et al. (2009), the magnetic fields were found to be stronger in younger HAeBe stars. They also observe that the strength of the magnetic field seems to be increasing with an increase in X-ray luminosity for HAe stars in their sample. The HAe stars are young ($\sim 1 - 2$ Myr), implying that the X-ray emission decays over time as the star reaches the Main Sequence. This agrees well with the model proposed by Tout & Pringle (1995), where a non-solar dynamo operates in rapidly rotating A-type stars based on rotational shear energy. Other possible mechanisms for X-ray emission from magnetic activity could be due to fossil fields or magnetically confined wind shocks (Babel & Montmerle 1997a). The HAeBe stars identified as

single stars in this paper (Table C1), are less studied and do not have enough data to understand their environment and companion status. This can be further explored with multi-wavelength photometry and spectrometry along with high-resolution spectro-polarimetric data to better understand the X-ray emission mechanism responsible for these stars. More evidence is required to support the origin of X-ray emission due to magnetic fields in HAeBe stars.

6 CONCLUSIONS

We present the X-ray analysis of a large sample of HAeBe stars, investigated with the *Chandra* X-ray telescope having a remarkable $\sim 1''$ spatial resolution. The main results obtained from this study are given below :

1. Out of 62 HAeBe sources, 44 have been detected in X-rays, i.e., a detection rate of $\sim 70.9\%$ is observed. We present new X-ray detections of 7 HAeBe stars in this work. The L_X of HAeBe stars ranges between 10^{28} to 10^{33} erg s^{-1} slightly higher than TTSS. The fractional X-ray luminosity of HAeBe stars ranges from $\log(L_X/L_{bol}) = -3.5$ to -10 , most of them falling between $\log(L_X/L_{bol}) = -4$ to -7 , which is in between the value observed for TTSS and OB-type MS stars.

2. In our sample, 25 out of 44 X-ray emitting HAeBe stars (56.2%) do not have any reported companions (the single status of some of the sources has been confirmed from previous high-resolution imaging studies). Some of the multi-star systems show variability and flaring, usually observed in TTSS. This evidence rules out the presence of low-mass companions as solely being the X-ray emitters in our sample of HAeBe stars.

3. The plasma temperatures of HAeBe stars without any known companions are in the soft energy regime ($kT \leq 2$ keV), differing from TTSS in which the hot component ($kT > 2$ keV) dominates. About 50% of non-single HAeBe stars fit with the 1T model and 80% of non-single HAeBe stars fit with the 2T model show hot X-ray emission, i.e., $kT > 2$ keV.

4. We do not find any correlation between the X-ray luminosity and the disk properties i.e., IR excess ($\eta_{2-4.6}$) and fractional accretion luminosity ($L_{H\alpha}/L_{bol}$) for the HAeBe stars in our sample, implying that the X-ray emission is not related to the dust content in the disk or accretion shocks.

5. From the X-ray spectrum and lightcurve analysis of the HAeBe stars in our sample, we see that the stars with confirmed low-mass companions have a plasma temperature on the hotter side following a similar pattern as TTSS. 9 stars are found to show variability/flaring features in the X-ray lightcurve. Such X-ray variability/flaring is not observed in single HAeBe stars and equal mass HAeBe star systems, except V892 Tau and V372 Ori.

From the results obtained, we propose that the X-ray emission from HAeBe is intrinsic and not due to the presence of a close low-mass companion. The X-rays from the HAeBe stars need to be studied further in-depth to constrain the emission mechanism. Studies by [Telleschi et al. \(2007b\)](#) and [Günther & Schmitt \(2009\)](#) suggest wind shock models and magnetically confined winds as possible mechanisms for X-ray emission. The validation of these models requires the presence of magnetic fields in HAeBe stars. Based on the previous studies on magnetic fields in literature we found that in single HAeBe stars (i.e., stars with no known sub-arcsec companion), structured magnetic fields could be present. This favors the sheer dynamo theory ([Tout & Pringle 1995](#)), fossil field hypothesis, or magnetically confined wind shocks ([Babel & Montmerle 1997a](#)). Further studies with multi-wavelength photometry and spectrometry

along with high-resolution spectro-polarimetric data are suggested to support the magnetically driven coronal emission model in these stars.

ACKNOWLEDGEMENTS

We thank the referee for providing constructive comments and suggestions that have helped enhance the quality of the paper. This research has made use of data obtained from the Chandra Data Archive and the software provided by the *Chandra* X-ray Center (CXC) in the application package “CIAO”. We also made use of the software “XSPEC” provided by the High Energy Astrophysics Science Archive Research Center (HEASARC), which is a service of the Astrophysics Science Division at NASA/GSFC. We thank the help desk at *Chandra* and HEASARC for clarifying doubts regarding the X-ray data analysis and software issues. This study has used the *Gaia* EDR3 data to obtain the distances for the sample of stars in this paper. Hence, we express our gratitude to the Gaia collaboration. We thank the SIMBAD database and VizieR online library service for helping with the relevant literature survey. We would like to thank our colleagues Dr. Savithri H Ezhikode, Ms. Nidhi Sabu, and Dr. Arun Roy for providing help with the X-ray and optical analysis part of the paper. We acknowledge the support given by the Center for Research, CHRIST (Deemed to be University), Bangalore, India. VJ and SSK thank the Inter-University Centre for Astronomy and Astrophysics (IUCAA), Pune, India, for the Visiting Associateship.

DATA AVAILABILITY

The data used in this work was accessed from the *Chandra* Data Archive (CDA; <https://cda.harvard.edu/chaser/mainEntry.do>).

REFERENCES

- Abt H. A., Wang R., Cardona O., 1991, *ApJ*, **367**, 155
Alecian E., et al., 2009, *MNRAS*, **400**, 354
Alecian E., et al., 2013, *MNRAS*, **429**, 1001
Alencar S. H. P., Melo C. H. F., Dullemond C. P., Andersen J., Batalha C., Vaz L. P. R., Mathieu R. D., 2003, *A&A*, **409**, 1037
Alonso-Albi T., Fuente A., Bachiller R., Neri R., Planesas P., Testi L., Berné O., Joblin C., 2009, *A&A*, **497**, 117
Andersen J., Lindgren H., Hazen M. L., Mayor M., 1989, *A&A*, **219**, 142
Appenzeller I., 1994, in The P. S., Perez M. R., van den Heuvel E. P. J., eds, *Astronomical Society of the Pacific Conference Series Vol. 62, The Nature and Evolutionary Status of Herbig Ae/Be Stars*. p. 12
Arnaud K. A., 1996, in Jacoby G. H., Barnes J., eds, *Astronomical Society of the Pacific Conference Series Vol. 101, Astronomical Data Analysis Software and Systems V*. p. 17
Arun R., Mathew B., Manoj P., Ujjwal K., Kartha S. S., Viswanath G., Narang M., Paul K. T., 2019, *The Astronomical Journal*, **157**, 159
Babel J., Montmerle T., 1997a, *A&A*, **323**, 121
Babel J., Montmerle T., 1997b, *ApJ*, **485**, L29
Bae J., Zhu Z., Hartmann L., 2016, *ApJ*, **819**, 134
Bailer-Jones C. A. L., Rybizki J., Fouesneau M., Demleitner M., Andrae R., 2021, *AJ*, **161**, 147
Baines D., Oudmaijer R. D., Porter J. M., Pozzo M., 2006, *MNRAS*, **367**, 737
Bevington P., Robinson D., 2003, *Data Reduction and Error Analysis for the Physical Sciences*. McGraw-Hill Education, <https://books.google.co.in/books?id=@poQAQAATAAJ>
Boccaletti A., et al., 2020, *A&A*, **637**, L5

- Boersma C., Peeters E., Martín-Hernández N. L., van der Wolk G., Verhoeff A. P., Tielens A. G. G. M., Waters L. B. F. M., Pel J. W., 2009, *A&A*, **502**, 175
- Bohlin R. C., Savage B. D., Drake J. F., 1978, *ApJ*, **224**, 132
- Böhm T., Catala C., Balona L., Carter B., 2004, *A&A*, **427**, 907
- Brittain S. D., Najita J. R., Carr J. S., 2019, *ApJ*, **883**, 37
- Brittain S. D., Kamp I., Meeus G., Oudmajer R. D., Waters L. B. F. M., 2023, *arXiv e-prints*, p. [arXiv:2301.01165](https://arxiv.org/abs/2301.01165)
- Calvet N., Gullbring E., 1998, *ApJ*, **509**, 802
- Caramazza M., Flaccomio E., Micela G., Reale F., Wolk S. J., Feigelson E. D., 2007, *A&A*, **471**, 645
- Carmona A., van den Ancker M. E., Henning T., 2007, *A&A*, **464**, 687
- Cazzoletti P., et al., 2018, *A&A*, **619**, A161
- Chauvin G., et al., 2003, *A&A*, **406**, L51
- Chen X. P., Henning T., van Boekel R., Grady C. A., 2006, *A&A*, **445**, 331
- Chen P. S., Shan H. G., Zhang P., 2016, *New Astron.*, **44**, 1
- Close L. M., et al., 1997, *ApJ*, **489**, 210
- Collins K. A., et al., 2009, *ApJ*, **697**, 557
- Corporon P., Lagrange A. M., 1999, *A&AS*, **136**, 429
- Corporon P., Lagrange A. M., Beust H., 1996, *A&A*, **310**, 228
- Currie T., et al., 2022, *Nature Astronomy*, **6**, 751
- D'Angelo G., Marzari F., 2022, *MNRAS*, **509**, 3181
- Da Rio N., Robberto M., Hillenbrand L. A., Henning T., Stassun K. G., 2012, *ApJ*, **748**, 14
- Daemgen S., Petr-Gotzens M. G., Correia S., Teixeira P. S., Brandner W., Kley W., Zinnecker H., 2013, *A&A*, **554**, A43
- Dahm S. E., Hillenbrand L. A., 2015, *AJ*, **149**, 200
- Damiani F., Micela G., Sciortino S., Harnden F. R. J., 1994, *ApJ*, **436**, 807
- Dong R., et al., 2022, *Nature Astronomy*, **6**, 331
- Dullemond C. P., Dominik C., 2004a, *A&A*, **417**, 159
- Dullemond C. P., Dominik C., 2004b, *A&A*, **421**, 1075
- Dullemond C. P., Dominik C., 2005, *A&A*, **434**, 971
- Dzib S., Loinard L., Mioduszewski A. J., Boden A. F., Rodríguez L. F., Torres R. M., 2010, *ApJ*, **718**, 610
- Espósito T. M., et al., 2020, *AJ*, **160**, 24
- Fairlamb J. R., Oudmajer R. D., Mendigutía I., Ilee J. D., van den Ancker M. E., 2015, *MNRAS*, **453**, 976
- Fairlamb J. R., Oudmajer R. D., Mendigutía I., Ilee J. D., van den Ancker M. E., 2017, *MNRAS*, **464**, 4721
- Fedele D., et al., 2017, *A&A*, **600**, A72
- Fedele D., Toci C., Maud L., Lodato G., 2021, *A&A*, **651**, A90
- Feigelson E. D., Broos P., Gaffney James A. I., Garmire G., Hillenbrand L. A., Pravdo S. H., Townsley L., Tsuboi Y., 2002, *ApJ*, **574**, 258
- Feigelson E. D., Gaffney James A. I., Garmire G., Hillenbrand L. A., Townsley L., 2003, *ApJ*, **584**, 911
- Flaccomio E., Micela G., Sciortino S., 2006, *A&A*, **455**, 903
- Forbrich J., Preibisch T., 2007, *A&A*, **475**, 959
- Forbrich J., Preibisch T., Menten K. M., 2006, *A&A*, **446**, 155
- Forbrich J., Osten R. A., Wolk S. J., 2011, *ApJ*, **736**, 25
- Freeman P. E., Kashyap V., Rosner R., Lamb D. Q., 2002, *ApJS*, **138**, 185
- Fruscione A., et al., 2006, in Silva D. R., Doxsey R. E., eds, Society of Photo-Optical Instrumentation Engineers (SPIE) Conference Series Vol. 6270, Society of Photo-Optical Instrumentation Engineers (SPIE) Conference Series. p. 62701V, doi:10.1117/12.671760
- Fuente A., Alonso-Albi T., Bachiller R., Natta A., Testi L., Neri R., Planesas P., 2006, *ApJ*, **649**, L119
- Fukagawa M., Tamura M., Itoh Y., Hayashi S. S., Oasa Y., 2003, *ApJ*, **590**, L49
- Fukagawa M., et al., 2004, *ApJ*, **605**, L53
- GRAVITY Collaboration et al., 2018, *A&A*, **620**, A116
- García P. J. V., et al., 2013, *MNRAS*, **430**, 1839
- Getman K. V., et al., 2005, *ApJS*, **160**, 319
- Getman K. V., Feigelson E. D., Lawson W. A., Broos P. S., Garmire G. P., 2008, *ApJ*, **673**, 331
- Getman K. V., Broos P. S., Kóspál Á., Salter D. M., Garmire G. P., 2016, *AJ*, **152**, 188
- Ghez A. M., McCarthy D. W., Patience J. L., Beck T. L., 1997, *ApJ*, **481**, 378
- Giardino G., Favata F., Micela G., Reale F., 2004, *A&A*, **413**, 669
- Giardino G., Favata F., Micela G., Sciortino S., Winston E., 2007, *A&A*, **463**, 275
- Godoy N., et al., 2022, *A&A*, **663**, A53
- Gómez de Castro A. I., López-Santiago J., Talavera A., Sytov A. Y., Bisikalo D., 2013, *ApJ*, **766**, 62
- Gómez de Castro A. I., Vallejo J. C., Canet A., Loyd P., France K., 2020, *ApJ*, **904**, 120
- Grady C. A., et al., 2007, *The Astrophysical Journal*, **665**, 1391
- Grady C. A., et al., 2010, *ApJ*, **719**, 1565
- Gratton R., et al., 2019, *A&A*, **623**, A140
- Greene T. P., Wilking B. A., Andre P., Young E. T., Lada C. J., 1994, *ApJ*, **434**, 614
- Grevesse N., Sauval A. J., 1998, *Space Sci. Rev.*, **85**, 161
- Guarcello M. G., et al., 2017, *A&A*, **602**, A10
- Günther H. M., Schmitt J. H. M. M., 2009, *A&A*, **494**, 1041
- Günther H. M., Schneider P. C., Li Z. Y., 2013, *A&A*, **552**, A142
- Haikala L. K., Olberg M., 2007, *A&A*, **466**, 191
- Haikala L. K., Reipurth B., 2010, *A&A*, **510**, A1
- Hamaguchi K., Yamauchi S., Koyama K., 2005, *ApJ*, **618**, 360
- Hamidouche M., Wang S., Looney L. W., 2008, *AJ*, **135**, 1474
- Hernández J., Calvet N., Briceño C., Hartmann L., Berlind P., 2004, *AJ*, **127**, 1682
- Hubrig S., et al., 2009, *A&A*, **502**, 283
- Hubrig S., et al., 2011, *Astronomische Nachrichten*, **332**, 1022
- Hubrig S., Ilyin I., Schöller M., Lo Curto G., 2013, *Astronomische Nachrichten*, **334**, 1093
- Imanishi K., Nakajima H., Tsujimoto M., Koyama K., Tsuboi Y., 2003, *PASJ*, **55**, 653
- Isella A., et al., 2018, *ApJ*, **869**, L49
- Järvinen S. P., Carroll T. A., Hubrig S., Schöller M., Ilyin I., Korhonen H., Pogodin M., Drake N. A., 2015, *A&A*, **584**, A15
- Järvinen S. P., Carroll T. A., Hubrig S., Ilyin I., Schöller M., Drake N. A., Pogodin M. A., 2019a, *MNRAS*, **486**, 5499
- Järvinen S. P., Carroll T. A., Hubrig S., Ilyin I., Schöller M., 2019b, *MNRAS*, **489**, 886
- Kastner J. H., Montez Rodolfo J., Rodriguez D., Grosso N., Zuckerman B., Perrin M. D., Forveille T., Graham J. R., 2010, *ApJ*, **719**, L65
- Kervella P., Arenou F., Mignard F., Thévenin F., 2019, *A&A*, **623**, A72
- Kirwan A., Murphy A., Schneider P. C., Whelan E. T., Dougados C., Eisloffel J., 2022, *A&A*, **663**, A30
- Kóspál Á., et al., 2012, *A&A*, **541**, A71
- Kuhn M. A., Getman K. V., Broos P. S., Townsley L. K., Feigelson E. D., 2013, *ApJS*, **209**, 27
- Lada C. J., 1987, *Symposium - International Astronomical Union*, **115**, 1–18
- Launhardt R., et al., 2020, *A&A*, **635**, A162
- Laws A. S. E., et al., 2020, *ApJ*, **888**, 7
- Leinendecker H., Jang-Condell H., Turner N. J., Myers A. D., 2022, *ApJ*, **941**, 172
- Leinert C., Richichi A., Haas M., 1997, *A&A*, **318**, 472
- Ligi R., et al., 2018, *MNRAS*, **473**, 1774
- Long F., et al., 2021, *ApJ*, **915**, 131
- Maheswar G., Manoj P., Bhatt H. C., 2002, *A&A*, **387**, 1003
- Maheswar G., Manoj P., Bhatt H. C., 2004, *MNRAS*, **355**, 1272
- Malfait K., Bogaert E., Waelkens C., 1998, *A&A*, **331**, 211
- Manoj P., Maheswar G., Bhatt H. C., 2002, *MNRAS*, **334**, 419
- Manoj P., Bhatt H. C., Maheswar G., Muneer S., 2006, *ApJ*, **653**, 657
- Manoj P., et al., 2011, *ApJS*, **193**, 11
- Mathew B., et al., 2018, *ApJ*, **857**, 30
- Matthews H. E., Purton C. R., Roger R. S., Dewdney P. E., Mitchell G. F., 2003, *ApJ*, **592**, 176
- Mayne N. J., 2010, *MNRAS*, **408**, 1409
- Mayne N. J., Naylor T., Littlefair S. P., Saunders E. S., Jeffries R. D., 2007, *MNRAS*, **375**, 1220
- McClure M., 2009, *ApJ*, **693**, L81
- McJunkin M., France K., Schneider P. C., Herczeg G. J., Brown A., Hillenbrand L., Schindhelm R., Edwards S., 2014, *ApJ*, **780**, 150
- Mesa D., et al., 2019, *A&A*, **624**, A4
- Millan-Gabet R., Monnier J. D., 2002, *ApJ*, **580**, L167

- Monnier J. D., Tannirkulam A., Tuthill P. G., Ireland M., Cohen R., Danchi W. C., Baron F., 2008, *ApJ*, **681**, L97
- Monnier J. D., et al., 2017, *ApJ*, **838**, 20
- Montmerle T., 2007, *Mem. Soc. Astron. Italiana*, **78**, 320
- Müller A., Carmona A., van den Ancker M. E., van Boekel R., Henning T., Launhardt R., 2011, *A&A*, **535**, L3
- Nazé Y., et al., 2011, *ApJS*, **194**, 7
- Núñez E. H., Povich M. S., Binder B. A., Townsley L. K., Broos P. S., 2021, *AJ*, **162**, 153
- Panić O., et al., 2021, *MNRAS*, **501**, 4317
- Pecaut M. J., Mamajek E. E., 2013, *ApJS*, **208**, 9
- Peres G., Orlando S., Reale F., 2004, *ApJ*, **612**, 472
- Pérez M. R., van den Ancker M. E., de Winter D., Bopp B. W., 2004, *A&A*, **416**, 647
- Pérez S., et al., 2020, *ApJ*, **889**, L24
- Petit V., Wade G. A., Drissen L., Montmerle T., Alecian E., 2008, *MNRAS*, **387**, L23
- Preibisch T., 1999, *A&A*, **345**, 583
- Preibisch T., Feigelson E. D., 2005, *ApJS*, **160**, 390
- Preibisch T., et al., 2005, *ApJS*, **160**, 401
- Pyerin M. A., Delage T. N., Kurtovic N. T., Gárate M., Henning T., Pinilla P., 2021, *A&A*, **656**, A150
- Racine R., 1968, *AJ*, **73**, 233
- Reipurth B., Zinnecker H., 1993, *A&A*, **278**, 81
- Rich E. A., et al., 2022, *AJ*, **164**, 109
- Rigliaco E., et al., 2023, *A&A*, **671**, A82
- Rodríguez L. F., Yam J. O., Carrasco-González C., Anglada G., Trejo A., 2016, *AJ*, **152**, 101
- Sallum S., Eisner J. A., Stone J. M., Dietrich J., Hinz P., Spalding E., 2021, *AJ*, **161**, 28
- Sandell G., Weintraub D. A., Hamidouche M., 2011, *ApJ*, **727**, 26
- Sandell G., Reipurth B., Vacca W. D., Bajaj N. S., 2021, *ApJ*, **920**, 7
- Sissa E., Gratton R., Alcalà J. M., Desidera S., Messina S., Mesa D., D'Orazi V., Rigliaco E., 2019, *A&A*, **630**, A132
- Skinner S. L., Güdel M., 2014, *ApJ*, **788**, 101
- Skinner S. L., Güdel M., Audard M., Smith K., 2004, *The Astrophysical Journal*, **614**, 221
- Smith R. K., Brickhouse N. S., Liedahl D. A., Raymond J. C., 2001, *The Astrophysical Journal*, **556**, L91
- Smith K. W., Balega Y. Y., Duschl W. J., Hofmann K. H., Lachaume R., Preibisch T., Schertl D., Weigelt G., 2005, *A&A*, **431**, 307
- Stecklum B., Eckart A., Henning T., Loewe M., 1995, *A&A*, **296**, 463
- Stelzer B., Flaccomio E., Montmerle T., Micela G., Sciortino S., Favata F., Preibisch T., Feigelson E. D., 2005, *ApJS*, **160**, 557
- Stelzer B., Micela G., Hamaguchi K., Schmitt J. H. M. M., 2006, *A&A*, **457**, 223
- Stelzer B., Robrade J., Schmitt J. H. M. M., Bouvier J., 2009a, *A&A*, **493**, 1109
- Stelzer B., Hubrig S., Orlando S., Micela G., Mikulášek Z., Schöller M., 2009b, *A&A*, **499**, 529
- Swartz D. A., Drake J. J., Elsner R. F., Ghosh K. K., Grady C. A., Wassell E., Woodgate B. E., Kimble R. A., 2005, *ApJ*, **628**, 811
- Tang Y. W., Guilloteau S., Piétu V., Dutrey A., Ohashi N., Ho P. T. P., 2012, *A&A*, **547**, A84
- Tang Y.-W., et al., 2017, *ApJ*, **840**, 32
- Telleschi A., Güdel M., Briggs K. R., Audard M., Palla F., 2007a, *A&A*, **468**, 425
- Telleschi A., Güdel M., Briggs K. R., Skinner S. L., Audard M., Franciosini E., 2007b, *A&A*, **468**, 541
- Testa P., Huenemoerder D. P., Schulz N. S., Ishibashi K., 2008, *ApJ*, **687**, 579
- Thomas S. J., Rodgers B., van der Blik N. S., Doppmann G., Bouvier J., Salvo C. A., Beuzit J. L., Rigaut F., 2023, *AJ*, **165**, 135
- Tout C. A., Pringle J. E., 1995, *MNRAS*, **272**, 528
- Townsley L. K., Broos P. S., Garmire G. P., Povich M. S., 2019, *ApJS*, **244**, 28
- Tsunemi H., Mori K., Miyata E., Baluta C., Burrows D. N., Garmire G. P., Chartas G., 2001, *ApJ*, **554**, 496
- Ubeira-Gabellini M. G., Christiaens V., Lodato G., Ancker M. v. d., Fedele D., Manara C. F., Price D. J., 2020, *ApJ*, **890**, L8
- Vioque M., Oudmaijer R. D., Baines D., Mendigutía I., Pérez-Martínez R., 2018, *A&A*, **620**, A128
- Wagner K., et al., 2018, *ApJ*, **854**, 130
- Wheelwright H. E., Oudmaijer R. D., Goodwin S. P., 2010, *MNRAS*, **401**, 1199
- Whelan E. T., Murphy A., Pascucci I., 2023, *ApJ*, **951**, 1
- Wichittanakom C., Oudmaijer R. D., Fairlamb J. R., Mendigutía I., Vioque M., Ababakr K. M., 2020, *MNRAS*, **493**, 234
- Williams P. M., Brand P. W. J. L., Longmore A. J., Hawarden T. G., 1977, *MNRAS*, **180**, 709
- Wilms J., Allen A., McCray R., 2000, *The Astrophysical Journal*, **542**, 914
- Winston E., et al., 2010, *AJ*, **140**, 266
- Zhekov S. A., Palla F., 2007, *MNRAS*, **382**, 1124
- Zhou Y., et al., 2022, *ApJ*, **934**, L13
- Zinnecker H., Preibisch T., 1994, *A&A*, **292**, 152
- van der Marel N., Verhaar B. W., van Terwisga S., Merín B., Herczeg G., Ligterink N. F. W., van Dishoeck E. F., 2016, *A&A*, **592**, A126

APPENDIX A: TABULATED PARAMETERS OF CHANDRA OBSERVATIONS OF HERBIG Ae/BE STARS

Table A1: Observation details of Herbig Ae/Be stars

SI No.	Object	X-ray Iden.	Obs ID	Instrument	RA (J2000)	Dec (J2000)	$A_V^{(a)}$	Distance(pc) ^(b)	No. of Obs.	Ref.
1	AB Aurigae	X	3755	ACIS-S	04:55:45.86	30:33:04.49	0.39	155.05 ± 0.81	1	10
2	AK Sco	X	combined ⁴	ACIS-I	16:54:44.85	-36:53:18.55	0.35	139.12 ± 0.57	3	4,10,23
3	AS 310	X	6399	ACIS-S	18:33:21.19	-04:58:05.78	6.06	2390.61 ± 77.58	1	13
4	BD+30 549	X	combined ⁵	ACIS-I	03:29:19.81	31:24:56.81	2.30	284.78 ± 1.93	3	4
5	AS 477	X2	6401	ACIS-S	21:52:34.10	47:13:43.60	2.00	756.28 ± 7.05	1	13
6	V361 Cep	X	6400	ACIS-S	21:42:50.22	66:06:35.08	2.78	882.79 ± 11.53	1	13
7	BD+65 1638	X2	6400	ACIS-S	21:42:58.84	66:06:10.21	3.39	1150 ± –	1	13
8	BP Psc	X	combined ⁶	ACIS-S	23:22:24.71	-02:13:41.76	1.34	211.39 ± 23.48	2	18
9	PDS 69	X2	6423	ACIS-I	13:57:43.92	-39:58:47.27	2.58	674.34 ± 7.63	1	11
10	V892 Tau	X2	3364	ACIS-S	04:18:40.62	28:19:15.54	11.99	133.06 ± 1.69	2	4,10
11	HD 100453	X2	6429	ACIS-S	11:33:05.63	-54:19:28.95	0.10	103.68 ± 0.22	1	15
12	HD 100546	X	combined ⁷	ACIS-I	11:33:25.39	-70:11:41.43	0.44	107.98 ± 0.42	2	4,10
13	HD 104237	X2	7326	ACIS-S	12:00:04.99	-78:11:34.66	0.59	106.48 ± 0.53	6	4,10
14	HD 141569	–	981	ACIS-I	15:49:57.70	-03:55:17.00	0.50	111.33 ± 0.37	1	4
15	HD 144432	X2	6398	ACIS-S	16:06:57.93	-27:43:10.09	0.53	154.16 ± 0.57	1	13
16	HD 147889	–	618	ACIS-I	16:25:24.32	-24:27:56.60	5.35	135.65 ± 0.42	1	4,10
17	HD 150193	X2	982	ACIS-I	16:40:17.95	-23:53:44.96	2.08	149.89 ± 0.41	1	4,10
18	HD 163296	X	12359	ACIS-S	17:56:21.29	-21:57:22.38	0.24	100.50 ± 0.34	2	4,10,20
19	HD 169142	X	6430	ACIS-S	18:24:29.79	-29:46:49.52	0.60	114.44 ± 0.30	1	7
20	HD 176386	–	3499	ACIS-I	19:01:38.90	-36:53:27.00	0.61	154.37 ± 0.64	8	9
21	HD 259431	X2	6397	ACIS-S	06:33:05.21	10:19:20.16	2.05	642.26 ± 11.33	1	13
22	HD 31648	X	8939	ACIS-S	04:58:46.27	29:50:36.64	0.55	155.08 ± 1.16	1	16
23	HD 97300	X	1867	ACIS-I	11:09:50.08	-76:36:47.65	2.15	188.78 ± 1.25	1	4
24	V373 Cep	–	6400	ACIS-S	21:43:06.68	66:06:54.60	5.14	870.73 ± 14.91	1	13
25	LkHa 25	–	2550	ACIS-I	06:40:44.60	09:48:02.00	1.98	694.02 ± 49.67	3	4
26	HD 36982	X	combined ⁸	ACIS-I	05:35:09.84	-05:27:52.95	1.32	404.00 ± 3.82	54	3
27	MR Ori	–	4373	ACIS-S	05:35:16.97	-05:21:45.33	2.58	395.34 ± 2.49	86	10
28	MWC 297	X2	1883	ACIS-I	18:27:39.54	-03:49:51.93	12.46	407.41 ± 5.19	1	4,10
29	PDS 144S	–	11012	ACIS-S	15:49:15.32	-26:00:54.70	0.92	1174.13 ± 119.29	1	*
30	PDS 581	–	4504	ACIS-S	19:36:18.90	29:32:50	4.24	1574.38 ± 208.99	1	*
31	R CrA	X	combined ⁹	ACIS-I	19:01:53.66	-36:57:08.01	5.45	126.02 ± 8.19	9	6
32	TY CrA	X	19709	ACIS-I	19:01:40.80	-36:52:34.01	2.84	159.13 ± 4.20	9	9
33	T CrA	X	combined ¹⁰	ACIS-I	19:01:58.79	-36:57:50.33	3.00	130.00 ± 0.00	7	9
34	HR 6000	X	9921	ACIS-I	16:08:34.55	-39:05:34.18	0.16	157.43 ± 1.05	13	13
35	HD 37062	X	4374	ACIS-I	05:35:31.42	-05:25:16.12	0.65	405.49 ± 6.45	67	1,2
36	V372 Ori	X	6418	ACIS-I	05:34:46.96	-05:34:15.15	0.84	447.95 ± 10.77	7	10
37	V380 Ori	X	12391	ACIS-S	05:36:25.40	-06:42:57.99	4.41	379.64 ± 15.06	2	4
38	HR 5999	X2	8901	ACIS-I	16:08:34.27	-39:06:18.34	0.54	157.67 ± 0.72	7	13
39	Z CMa	X	10845	ACIS-S	07:03:43.16	-11:33:06.24	7.89	639.94 ± 222.48	2	4,14
40	HBC 217	X	2540	ACIS-I	06:40:42.18	09:33:37.26	0.29	703.07 ± 6.98	7	25
41	HBC 442	X	combined ¹¹	ACIS-S	05:34:14.16	-05:36:54.38	0.38	383.52 ± 2.58	3	*
42	HD 135344 B	X	9927	ACIS-S	15:15:48.44	-37:09:16.34	0.37	134.55 ± 0.46	1	22
43	HBC 222	X	2550	ACIS-S	06:40:51.20	09:44:46.00	0.18	704.58 ± 6.86	3	21
44	HD 135344	–	9927	ACIS-S	15:15:48.90	-37:08:56.00	0.36	134.18 ± 0.58	1	*
45	LkHa 257	–	15723	ACIS-I	21:54:18.80	47:12:10.00	2.28	786.10 ± 8.13	1	*
46	LkHa 260	–	978	ACIS-I	18:19:09.40	-13:50:41.00	5.16	1556.18 ± 89.85	5	*
47	LkHa 339	–	12392	ACIS-I	06:10:57.80	-06:14:40.00	4.15	824.55 ± 10.46	1	*
48	MWC 930	–	23646	ACIS-I	18:26:25.20	-07:13:18.00	14.06	7129.11 ± 2189.23	1	*
49	RR Tau	–	8242	ACIS-I	05:39:30.50	26:22:27.00	3.62	798.19 ± 18.67	1	*
50	GSC 3975-0579	–	16309	ACIS-S	21:38:08.50	57:26:48.00	1.26	901.56 ± 13.67	2	*
51	HD 36939	X	4396	ACIS-S	05:34:55.29	-05:30:22.09	0.81	416.48 ± 7.24	45	1,2

⁴ AK Sco: 983+13274+13275⁵ BD+30 549: 642+6436+6437⁶ BP PSc: 10856+8900⁷ HD 100546: 2403+3427⁸ HD 36982: 4395+3744+4373+4374+4396+3498+17735⁹ R CrA: 19+3499+4475+5402+5403+5404+5405+19709¹⁰ T CrA: 19+5404¹¹ HBC 442: 6416+6417+8936

Table A1: Observation details of Herbig Ae/Be stars

SI No.	Object	X-ray Iden.	Obs ID	Instrument	RA (J2000)	Dec (J2000)	$A_V^{(a)}$	Distance(pc) ^(b)	No. of Obs.	Ref.
52	HD 250550	X	21185	ACIS-S	06:02:00.00	16:30:57	0.70	748.41 ± 25.88	1	*
53	R Mon	X	21183	ACIS-S	06:39:09.95	08:44:09.55	5.66	800.00 ± 0.00	1	*
54	HD 244604	X	21187	ACIS-S	05:31:57.23	11:17:41.52	1.69	397.93 ± 3.33	1	*
55	V346 Ori	–	21186	ACIS-S	05:24:42.80	01:43:48.00	0.31	336.39 ± 2.39	2	*
56	[DLM2010] EC 95a	X	4479	ACIS-I	18:29:57.89	01:12:46.15	36.00	429.20 ± 2.00	1	8
57	T Ori	–	2567	ACIS-S	05:35:50.50	-05:28:35.00	2.54	398.95 ± 4.90	25	*
58	MWC 953	X	2298	ACIS-I	18:43:28.42	-03:46:17.03	5.84	1985.43 ± 68.25	1	*
59	PDS 37	–	7519	ACIS-S	10:10:00.32	-57:02:07.35	9.37	1626.95 ± 63.06	1	*
60	HD 190073	X	21184	ACIS-S	20:03:02.51	05:44:16.65	0.34	824.88 ± 21.93	1	*
61	HD 245906	X	8242	ACIS-I	05:39:30.47	+26:19:55.15	1.11	900.58 ± 296.13	1	*
62	AFGL 961	X	12142	ACIS-I	06:34:37.74	04:12:44.20	32.00	1500.00 ± 0.00	1	21

“–” in column (3) denotes non-detections. “*” in column (11) denotes new stars which are not previously studied.

Table A1: (a) The A_V values were compiled from [Preibisch \(1999\)](#), [Hamaguchi et al. \(2005\)](#), [Stelzer et al. \(2006\)](#), [Manoj et al. \(2006\)](#), [Stelzer et al. \(2009a\)](#), [Dahm & Hillenbrand \(2015\)](#), [Fairlamb et al. \(2015\)](#), [Mathew et al. \(2018\)](#), [Vioque et al. \(2018\)](#) and [Arun et al. \(2019\)](#).

(b) Distance measurements were compiled from [Preibisch \(1999\)](#), [Manoj et al. \(2006\)](#), [Sandell et al. \(2011\)](#), [\(Dahm & Hillenbrand 2015\)](#) and [Bailer-Jones et al. \(2021\)](#).

References: (1) [Feigelson et al. \(2002\)](#), (2) [Feigelson et al. \(2003\)](#), (3) [Getman et al. \(2005\)](#), (4) [Stelzer et al. \(2006\)](#), (5) [Flaccomio et al. \(2006\)](#), (6) [Forbrich et al. \(2006\)](#), (7) [Grady et al. \(2007\)](#), (8) [Giardino et al. \(2007\)](#), (9) [Forbrich & Preibisch \(2007\)](#), (10) [Hamidouche et al. \(2008\)](#), (11) [Getman et al. \(2008\)](#), (12) [Testa et al. \(2008\)](#), (13) [Stelzer et al. \(2009a\)](#), (14) [Stelzer et al. \(2009b\)](#), (15) [Collins et al. \(2009\)](#), (16) [Grady et al. \(2010\)](#), (17) [Winston et al. \(2010\)](#), (18) [Kastner et al. \(2010\)](#), (19) [Forbrich et al. \(2011\)](#), (20) [Günther et al. \(2013\)](#), (21) [Kuhn et al. \(2013\)](#), (22) [McJunkin et al. \(2014\)](#), (23) [Getman et al. \(2016\)](#), (24) [Guarcello et al. \(2017\)](#), (25) [Townsend et al. \(2019\)](#).

APPENDIX B: X-RAY PARAMETERS OF HAEBE STARS

Table B1: X-ray parameters of HAeBe Stars from the Model Fitting

Name	N_H [10^{22} cm $^{-2}$]	kT1 [keV]	kT2 [keV]	statistic	P_{null}	GOF	χ^2	χ_{red}^2	DOF	log L_X [erg s $^{-1}$]
AB Aurigae	0.05	0.78±0.13		c		53.00%			10	29.11±0.10
AK Sco	0.04	0.59±0.14		c		31.00%			8	29.10±0.09
AS 310	0.70	0.57±0.33		c		52.00%			4	31.00±0.24
BD+30 549	2.22±1.04	0.23±0.14		χ^2	5.87E-01		1.93	0.64	3	31.29±1.22
V361 Cep	0.32	1.54±0.56		c		22.00%			12	30.56±0.10
BP Psc	7.94	2.07±19.15		c		3.00%			7	29.17±0.49
HD 100546	0.05	1.40±0.44		c		9.00%			9	29.21±0.10
HD 163296	0.18±0.05	0.12±0.04	0.58±0.04	χ^2	1.40E-01		83.94	1.18	71	29.89±0.14
HD 169142	0.07	0.21±0.02		c		39.00%			13	29.19±0.09
HD 31648	0.52±0.25	0.48±0.16		χ^2	1.74E-01		7.69	1.538	5	29.91±0.36
HD 97300	0.12±0.06	2.50±0.38		χ^2	2.45E-02		77.49	1.41	55	29.87±0.03
HD 36982	0.15	1.06±0.22		χ^2	2.79E-01		10.96	1.22	9	28.58±0.07
R CrA	0.63			PIMMS						29.85±0.06
TY CrA	0.33	1.41±0.15	8.25±3.23	χ^2	2.21E-01		341.2	1.06	322	31.45±0.02
HR 6000	0.02	0.74±0.09	1.29±0.24	χ^2	2.01E-01		72.15	1.15	63	30.15±0.02
HD 37062	0.23±0.03	1.01±0.07	2.75±0.22	χ^2	2.61E-02		177.63	1.24	143	31.12±0.02
V372 Ori	0.10	0.94±0.21	3.47±0.80	χ^2	4.64E-01		71.41	1.01	71	30.96±0.03
V380 Ori	1.05±0.13	0.45±0.11	4.32±2.95	χ^2	7.46E-02		123.27	1.21	102	31.91±0.18
Z CMa	0.92	0.66±0.20		χ^2	2.90E-01		6.17	1.23	5	30.62±0.34
HBC 217	0.03	0.98±0.11		χ^2	5.14E-01		6.23	0.89	7	29.95±0.06
HBC 442	0.04	0.86±0.12		χ^2	1.73E-01		16.4	1.37	12	29.80±0.06
HD 135344B	0.04	0.20±0.14	0.74±0.07	χ^2	7.94E-01		29.79	0.81	37	29.55±0.03
HD 36939	0.09	0.93±0.11		χ^2	2.65E-01		13.46	1.22	11	29.65±0.06
HD 250550	0.08	1.02±0.54		c		38.00%			3	30.15±0.30
HD 244604	0.20			PIMMS						29.18±0.26
HD 245906	0.13	0.65±0.35		χ^2	5.92E-01		1.91	0.64	3	30.75±0.35
R Mon	0.66			PIMMS						30.76±0.15
AFGL 961	22.89±15.31	1.13±1.49		χ^2	4.54E-01		2.62	0.87	3	33.12±1.39
[DLM2010] EC 95a	3.59±0.18	3.05±0.26		χ^2	7.90E-01		175.99	0.92	192	31.79±0.03
HBC 222	0.02	0.65±0.32		c		16.00%			9	30.08±0.11
MWC 953	0.68			PIMMS						30.64±0.27
HD 190073	0.04			PIMMS						29.86±0.34

Table B1: X-ray parameters of HAeBe Stars from the Model Fitting

Name	$N_H [10^{22} \text{ cm}^{-2}]$	kT1 [keV]	kT2 [keV]	statistic	P_{null}	GOF	χ^2	χ_{red}^2	DOF	$\log L_X [\text{erg s}^{-1}]$
T CrA	0.35			PIMMS						28.35±0.25
AS 477 A	0.23	1.53±3.26		c		13.00%			4	29.71±0.23
BD+65 1638 A	0.39	1.98±0.59		χ^2	5.06E-01		9.28	0.928	10	31.23±0.05
PDS 69 A	0.30	1.56±0.59		c		41.00%			10	30.20±0.10
V892 Tau A	1.06±0.17	2.07±0.30		χ^2	1.41E-01		80.61	1.19	68	30.61±0.06
HD 100453 A	0.01	0.27±0.05		c		3.00%			6	28.68±0.12
HD 104237 A	0.36±0.11	0.34±0.05	1.91±0.30	χ^2	6.03E-02		82.43	1.29	64	30.91±0.17
HD 144432 A	0.06	0.57±0.14		c		13.00%			8	29.04±0.10
HD 150193 A	0.24	0.87±0.49		c		13.00%			3	29.47±0.26
HD 259431 A	0.24	2.51±0.91		χ^2	3.17E-01		10.43	1.16	9	30.98±0.07
MWC 297 A	1.45	1.84±2.39		c		2.00%			8	29.56±0.18
HR 5999 A	0.06			PIMMS						28.91±0.23
AS 477 B	0.23	1.48±0.72		c		47.00%			14	30.37±0.10
BD+65 1638 B	0.39	1.13±0.10		χ^2	6.40E-02		26.61	1.57	17	31.40±0.04
PDS 69 B	0.30			PIMMS						30.07±0.16
V892 Tau B	1.39	1.16±0.26		χ^2	3.84E-01		8.53	1.07	8	29.99±0.12
HD 100453 B	0.01	0.73±0.22		c		36.00%			7	28.68±0.10
HD 104237 B	0.07	0.64±0.15		c		13.00%			9	29.17±0.11
HD 144432 B	0.03±0.02	0.85±0.11	3.23±0.65	χ^2	7.53E-02		102.17	1.23	83	30.35±0.04
HD 150193 B	0.24	1.40±0.26		χ^2	3.61E-01		7.69	1.10	7	30.29±0.07
HD 259431 B	0.24	1.02±0.30		c		27.00%			7	30.42±0.12
MWC 297 B	1.45			PIMMS						29.69±0.21
HR 5999 B	0.06	1.04±0.10	>5.75	χ^2	1.73E-01		40.51	1.23	33	30.36±0.05
HD 176386 B	0.07	0.88±0.08	1.68±0.34	χ^2	1.50E-01		100.68	1.16	87	30.30±0.02
V373 Cep B	0.60			PIMMS						30.29±0.18

Table B2: Upper-limits for L_X of non-detected sources in X-rays

Sl. No	Name	$N_H [10^{22} \text{ cm}^{-2}]$	$\log L_X [\text{erg s}^{-1}]$
1	HD 141569 A	0.06	< 28.75
2	HD 147889	0.62	< 28.65
3	V373 Cep A	0.60	< 29.93
4	LkHa 25	0.23	< 29.26
5	MR Ori	0.30	< 29.15
6	PDS 144 S	0.11	< 27.79
7	PDS 581	0.49	< 30.40
8	PDS 37	1.09	< 31.17
9	HD 176386 A	0.07	< 27.92
10	HD 135344	0.04	< 28.11
11	LkHa 257	0.27	< 29.17
12	LkHa 260	0.60	< 30.32
13	LkHa 339	0.48	< 29.15
14	MWC 930	1.63	< 32.01
15	RR Tau	0.42	< 29.58
16	GSC 3975-0579	0.15	< 30.29
17	V346 Ori	0.04	< 28.94
18	T Ori	0.30	< 29.83

Table B1: Column(1) provides the name of the object, Column(2) the absorption column density in 10^{22} cm^{-2} units, Column(3) & (4) the plasma temperature in keV, Column(5) identifies the test statistic used for model fitting, Column(6)(7)(8)(9) & (10) gives the null-hypothesis value, goodness of fit, χ^2 , χ_{red}^2 and degrees of freedom, finally Column(11) gives L_X in log scale. Table B2: “<” denotes that the value is upper-limit.

APPENDIX C: DETAILS OF THE COMPANION STATUS OF X-RAY EMITTING STARS

Table C1: Details of H AeBe stars detected in X-rays

Object	SpT	Binary	Resolved in <i>Chandra</i> (Sep")	Details of companion	Reference
AB Aurigae	A0	No	–	Planetary companion (<1")	69, 73
AK Sco	F5	Yes	No	Stellar companion (F5-type; <1")	12, 39, 57
AS 310	B1	No	–	–	75
BD+30 549	B8	No	–	–	
V361 Cep	B2	No	–	–	
BP Psc	G9	Yes	No	Stellar companion (<1")	31
HD 100546	B9	No	–	Planetary companion (<1")	50, 60, 62, 63
HD 163296	A0	No	–	Planetary companion (<1")	47, 70, 71
HD 169142	B9	No	–	Planetary companion (<1")	43, 44, 48, 51
HD 31648	A5	No	–	–	75
HD 97300	B9V	Yes	No	Stellar companion M3.5-type (<1")	7, 36, 37
HD 36982	B2	No	–	–	
R CrA	A5	Yes	No	Stellar companions equal mass star ($\sim 2.3M_{\odot}$; <1") +M-type ($\sim 0.156M_{\odot}$)	54, 55, 58, 66
TY CrA	B9	Yes	No	Quadruple star system K2+F-type (<1.2 AU; <1") M4-type (~ 41 AU; ~ 0.3 ")	4, 13, 21, 27
T CrA	F0	Yes	No	Stellar companion ($\sim 1M_{\odot}$; <1")	74, 76
HR 6000	A1.5	–	–	Unknown companion ($\sim 52M_{Jup}$; <1")	53
HD 37062	B4	Yes	No	Triple star system 2 stars (LMS+A-type; <1")	8, 46
V372 Ori	B9.5	Yes	No	Stellar companion Spectroscopic binary; A0.5-type	1, 10
V380 Ori	A1	Yes	No	Quadruple system TTS+IR source (<1") M5 type (>1")	26, 42
Z CMa	B5+F5	Yes	No	Stellar companion FU Ori (<1")	11, 67
HBC 217	G0	No	–	–	75
HBC 442	F8	No	–	–	
HD 135344B	A0	No	–	Planetary companion (<1")	41, 45
HD 36939	B8-B9	No	–	–	
HD 250550	B9	Yes	No	Stellar companion LMS ($\sim 0.8M_{\odot}$; <1")	59, 72
HD 244604	A0	No	–	–	75
HD 245906	A6	Yes	No	Stellar companion G5-type (<1")	33
R Mon	B8 IIIe	Yes	No	Stellar companion TTS (<1")	5, 20
AFGL 961	B2-B3/B5	Yes	–	Stellar companion early B-type (>1")	35
[DLM2010] EC 95a	K2	Yes	No	Stellar companion TTS (<1")	30
HBC 222	F8	No	–	–	75
MWC 953	B2Ve	No	–	–	75
V1295 Aql	A2IVe	No	–	Planetary companion (<1")	72
AS 477	A0	Yes	Yes (1.4")	Stellar companion Visual companion (>1")	9, 28
BD+65 1638	B2	Yes	Yes (1.332")	Stellar companion B-type (>1")	28, 40
PDS 69	B7	Yes	Yes (3.774")	Stellar companion B4-type (possible H AeBe ; >1")	2, 15, 22, 32

Table C1: Details of H Ae Be stars detected in X-rays

Object	SpT	Binary	Resolved in <i>Chandra</i> (Sep ^{''})	Details of companion	Reference
V892 Tau	A0	Yes	Yes (4.523 ^{''})	Stellar companion A-type (<1 ^{''}) + M3-type (>1 ^{''})	24, 61
HD 100453	A9Ve	Yes	Yes (1.007 ^{''})	Planetary companion (<1 ^{''}) + M-dwarf (~1 ^{''})	18, 29, 49
HD 104237	A4	Yes	Yes (1.482 ^{''})	Stellar companion K3 (<1 ^{''}) + M3/M4-type (>1 ^{''})	16, 25, 38, 52, 68
HD 144432	A8	Yes	Yes (1.400 ^{''})	Stellar companion K7+M1-type (>1 ^{''})	17, 23, 34
HD 150193	A0	Yes	Yes (1.406 ^{''})	Stellar companion K4-type (>1 ^{''})	2, 14, 44
HD 259431	B6	Yes	Yes (3.112 ^{''})	Stellar companion ~0.6 M _⊙ source (<1 ^{''}) Visual companion (>1 ^{''})	19, 33, 72
MWC 297	B1	Yes	Yes (3.532 ^{''})	Stellar companion low mass star (<1 ^{''} ; ~0.1-0.5M _⊙) Visual companion (>1 ^{''})	56, 64, 72
HR 5999	A7	Yes	Yes (1.574 ^{''})	Stellar companion TTS (>1 ^{''})	3, 6, 65, 72

References: (1) Abt et al. (1991), (2) Reipurth & Zinnecker (1993), (3) Stecklum et al. (1995), (4) Corporon et al. (1996), (5) Ghez et al. (1997), (6) Close et al. (1997), (7) Leinert et al. (1997), (8) Corporon & Lagrange (1999), (9) Maheswar et al. (2002), (10) Manoj et al. (2002), (11) Millan-Gabet & Monnier (2002), (12) Alencar et al. (2003), (13) Chauvin et al. (2003), (14) Fukagawa et al. (2003), (15) (Maheswar et al. 2004), (16) Böhm et al. (2004), (17) Pérez et al. (2004), (18) Chen et al. (2006), (19) Baines et al. (2006), (20) Fuente et al. (2006), (21) Forbrich & Preibisch (2007), (22) Haikala & Olberg (2007), (23) Carmona et al. (2007), (24) Monnier et al. (2008), (25) Testa et al. (2008), (26) Alecian et al. (2009), (27) Boersma et al. (2009), (28) Stelzer et al. (2009a), (29) Collins et al. (2009), (30) Dzib et al. (2010), (31) Kastner et al. (2010), (32) Haikala & Reipurth (2010), (33) Wheelwright et al. (2010), (34) Müller et al. (2011), (35) Sandell et al. (2011), (36) Kóspál et al. (2012), (37) Daemgen et al. (2013), (38) Garcia et al. (2013), (39) Gómez de Castro et al. (2013), (40) Dahm & Hillenbrand (2015), (41) Bae et al. (2016), (42) Rodríguez et al. (2016), (43) Fedele et al. (2017), (44) Monnier et al. (2017), (45) Cazzoletti et al. (2018), (46) GRAVITY Collaboration et al. (2018), (47) Isella et al. (2018), (48) Ligi et al. (2018), (49) Wagner et al. (2018), (50) Brittain et al. (2019), (51) Gratton et al. (2019), (52) Järvinen et al. (2019a), (53) Kervella et al. (2019), (54) Mesa et al. (2019), (55) Sissa et al. (2019), (56) Ubeira-Gabellini et al. (2020), (57) Gómez de Castro et al. (2020), (58) Launhardt et al. (2020), (59) Laws et al. (2020), (60) Fedele et al. (2021), (61) Long et al. (2021), (62) Pérez et al. (2020), (63) Pyerin et al. (2021), (64) Sallum et al. (2021), (65) Panić et al. (2021), (66) Sandell et al. (2021), (67) Dong et al. (2022), (68) Godoy et al. (2022), (69) Currie et al. (2022), (70) D'Angelo & Marzari (2022), (71) Leiendecker et al. (2022), (72) Rich et al. (2022), (73) Zhou et al. (2022), (74) Rigliaco et al. (2023), (75) Thomas et al. (2023), (76) Whelan et al. (2023).

APPENDIX D: H AEBE STARS: VARIABLE LIGHTCURVES

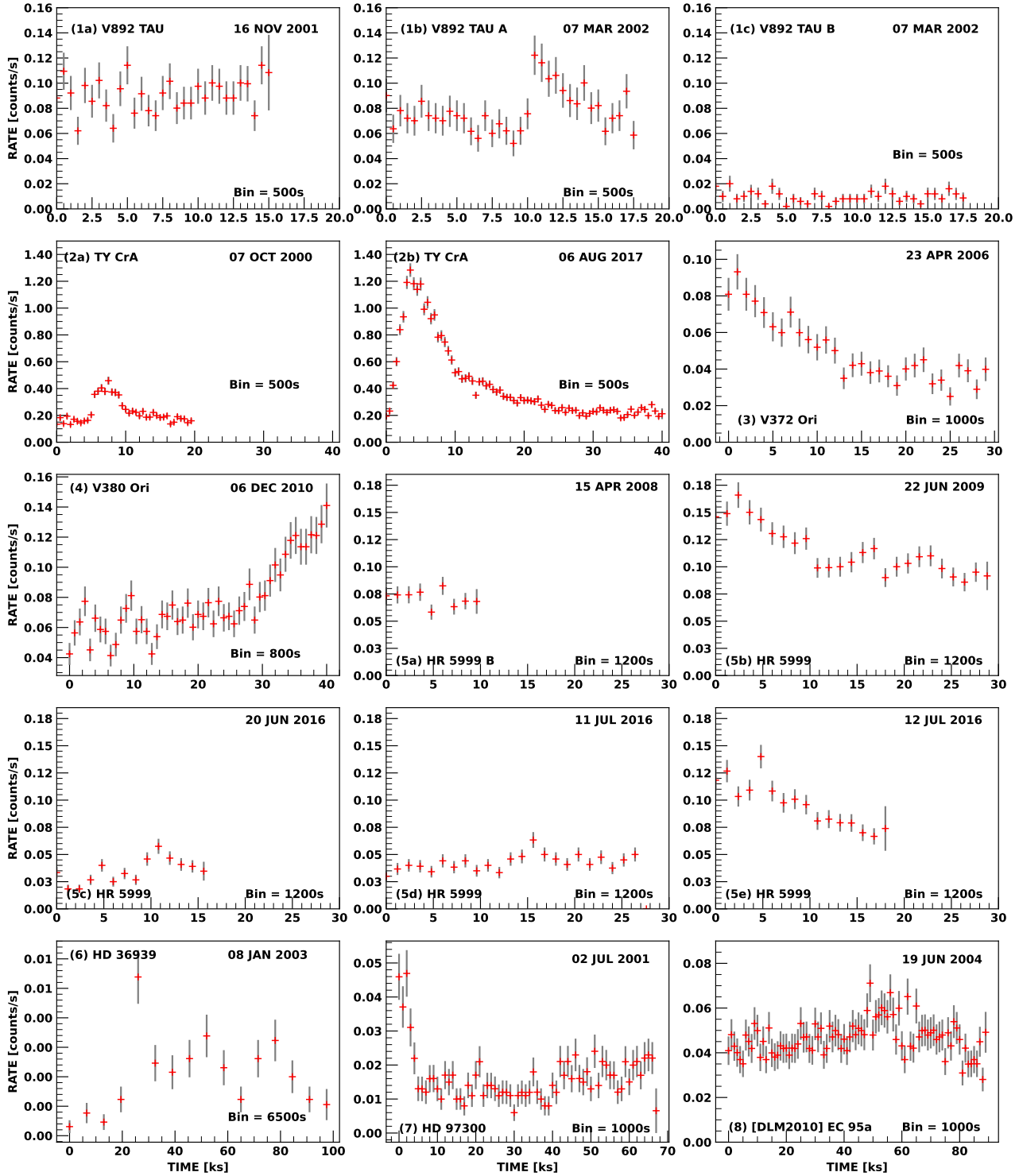


Figure D1. *Chandra* ACIS lightcurves of 8 stars in the energy range 0.3 – 8.0 keV that present variability and flaring. The fixed bin time in seconds for each source is mentioned at the bottom right of the plot.

This paper has been typeset from a \LaTeX file prepared by the author.

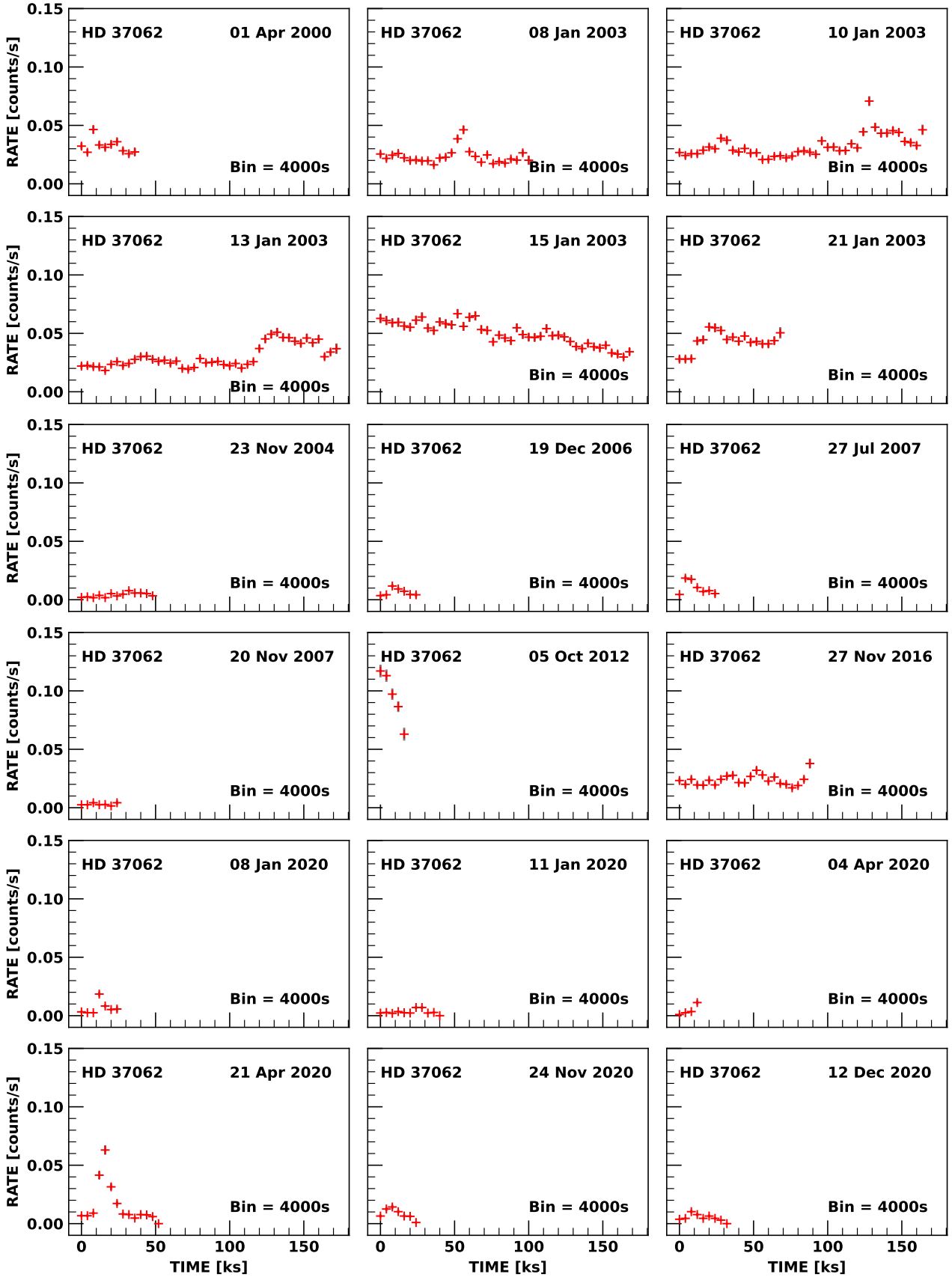


Figure D2. *Chandra* ACIS lightcurves of HD 37062 in the energy range 0.3 – 8.0 keV presenting variability and flaring over a period of 20 years. The fixed bin time in seconds for each source is mentioned at the bottom right of the plot.